



HAL
open science

PCM-modified textile-reinforced concrete slab: A multiscale and multiphysics investigation

Zakaria Ilyes Djamai, Khuong Le Nguyen, Amir Si Larbi, Ferdinando Salvatore, Gaochuang Cai

► **To cite this version:**

Zakaria Ilyes Djamai, Khuong Le Nguyen, Amir Si Larbi, Ferdinando Salvatore, Gaochuang Cai. PCM-modified textile-reinforced concrete slab: A multiscale and multiphysics investigation. Construction and Building Materials, 2021, 293, pp.123483. 10.1016/j.conbuildmat.2021.123483 . hal-03332382

HAL Id: hal-03332382

<https://hal.insa-toulouse.fr/hal-03332382>

Submitted on 24 May 2023

HAL is a multi-disciplinary open access archive for the deposit and dissemination of scientific research documents, whether they are published or not. The documents may come from teaching and research institutions in France or abroad, or from public or private research centers.

L'archive ouverte pluridisciplinaire **HAL**, est destinée au dépôt et à la diffusion de documents scientifiques de niveau recherche, publiés ou non, émanant des établissements d'enseignement et de recherche français ou étrangers, des laboratoires publics ou privés.



Distributed under a Creative Commons Attribution - NonCommercial 4.0 International License

1 ***PCM-modified textile-reinforced concrete slab: A multiscale and multiphysics***
2 ***investigation***

3 Zakaria Ilyes Djamaï¹, Khuong Le Nguyen², Amir Si Larbi³, Ferdinando Salvatore³,
4 Gaochuang Cai³

5 1-LMDC (Laboratoire Matériaux et Durabilité des Constructions), Université de Toulouse,
6 INSA/UPS Génie Civil, 135 Avenue de Rangueil, 31077 Toulouse cedex 04, France.

7 2-Faculty of Civil Engineering, University of seven Transport Technology, Hanoi, Vietnam

8 3-Université de Lyon, Ecole Nationale d'Ingénieurs de Saint-Etienne (ENISE), Laboratoire de
9 Tribologie et de Dynamique des Systèmes (LTDS), 58 Rue Jean Parot, 42000 Saint-Etienne,
10 France

11 Corresponding author: djamaï@insa-toulouse.fr

12 **Abstract**

13 This paper presents a multiphysics investigation of the effectiveness of textile-reinforced
14 concrete (TRC) composite modified by the addition of phase change materials (PCMs).

15

16 The potential of this composite lies in the combination of the lightweight characteristic of
17 TRC with the heat storage capacities provided by PCMs.

18

19 This study focuses on the effects of PCMs on both the mechanical and thermal performances
20 of TRCs. The efficiency of an innovative concept of PCM–TRC slab resulting from the
21 reinforcement of a PCM modified matrix with a textile grid is mechanically and thermally
22 evaluated.

23 Despite the degradation of the mechanical performance of PCM–TRC slabs with PCM
24 content, the ductile and multicracking behaviors of the slabs are conserved.

25 The temperature and thus the PCM state (solid or liquid) affect the mechanical performance
26 of the PCM–mortar matrix and PCM–TRC slabs. This can be attributed to the PCM volume
27 change that occurs during phase change.

28 In terms of thermal performance, in comparison with the reference TRC slab, the 10wt%
29 PCM–TRC slab (4.5 cm thick) results in an energy saving of 37% and a temperature decrease
30 of 4°C at the peak.

31 **Key words**

32 Phase change material (PCM), textile-reinforced concrete (TRC), mechanical behavior,
33 thermal behavior, physicochemical investigation

34 **1-Introduction**

35 The building industry is one of the many consumers of energy. In the European Union, this
36 industry accounts for 40% of the total energy consumption and 37% of the CO₂ emissions [1].

1 The use of renewable energy resources is crucial for improving building efficiency. In this
2 context, the use of composite and non-conventional materials is increasing worldwide.

3
4 Textile-reinforced concrete (TRC) comprises a fine aggregate cementitious matrix reinforced
5 with a non-corrosive textile fabric [2, 3]. TRC allows for the combination of compressive
6 resistance and tensile strength due to textile reinforcement, thus enabling the construction of
7 lightweight elements, such as sandwich and cladding panels [4, 5, 6, 7 and 8]. TRC exhibits a
8 significant resistance to temperature (such as situations involving fire) and is considered as a
9 promising alternative to fibre-reinforced polymers, which are characterised by their expensive
10 cost, fire instability, and toxicity [6]. Despite these benefits, the reduced thickness of TRC
11 structures (which are lightweight because of the reduced covers attributed to the non-
12 corrosive fabric) can lead to the degradation of thermal inertia, thus limiting the possibilities
13 of current construction applications.

14 Although sensible heat storage is the most exploited in the construction industry owing to the
15 wide range of building materials, such as concrete and cellular foams, latent heat storage with
16 the incorporation of phase change materials (PCMs) is of growing interest in the scientific
17 community. PCM can reduce the indoor temperature variation by absorbing and releasing the
18 latent heat generated by a phase change in a narrow temperature range [9, 10]. When the
19 temperature is above the phase change temperature, the PCM melts and absorbs energy that
20 can be restored when the PCM solidifies at a temperature below the phase change
21 temperature.

22 The incorporation of PCM in cementitious materials, such as concrete, has received
23 significant attention from researchers through different techniques, such as direct
24 incorporation [11, 12], shape stabilisation [13], and vacuum impregnation [14]. However, the
25 encapsulation technique [15, 16, 17, 18, 19, and 20] is the most suitable for preventing
26 leakage of pure PCM wax.

27 Several researchers have investigated the incorporation of encapsulated PCM in concrete to
28 achieve thermal comfort in the building envelope. Some researchers [19, 21, 22, and 23]
29 studied the energy saving of PCM-concrete without analysing the effect of PCM on the
30 microstructure and mechanical behaviour of concrete. Other researchers [24, 25] focused
31 more on the mechanical behaviour of PCM-concrete structures without evaluating the effect
32 of PCM on thermal performances. Other research studies [26, 27] focused on the effect of
33 PCM on the mechanism of cement hydration and its consequences on the microstructure of
34 concrete.

35 Castellon [19] constructed two identical cubicles (with walls having a 12-cm thickness)
36 composed of plain concrete and PCM-modified concrete containing 5wt% PCM. These
37 cubicles were located in the south of Spain and were exposed to the atmosphere. The PCM-
38 concrete cubicles demonstrated a peak temperature attenuation of 4°C with a peak delay time
39 of 4 h. Hunger [20] observed a 12% energy saving using self-compacting concrete containing
40 5wt% microencapsulated PCM when subjected to cyclic thermal loading. Although the
41 thermal benefits of PCM addition in concrete have been verified in the literature [21, 22],

1 negative effects of PCM addition are also observed in the mechanical performance of PCM-
2 concrete [24, 25, 26, 27, 28]. In addition, the high costs of the PCM encapsulation process, as
3 well as steel reinforcement, lead to uncompetitive steel-reinforced PCM concrete, which
4 further hinders the introduction of PCM concrete in the construction market. Furthermore,
5 PCM can significantly increase the porosity and critical pore diameter of concrete [29],
6 thereby reducing its durability, particularly in the case of an association with corrosive steel
7 reinforcement.

8 The present study aims to enrich the state of the art on the effect of PCM addition on the
9 thermomechanical behaviour of concrete and to combine the advantages of PCM-modified
10 concrete and TRC to propose a new PCM-modified TRC composite ‘PCM–TRC’. **The**
11 **purpose of this study is to evaluate the efficiency of the proposed composite in structural**
12 **elements, such as slabs.**

13 The concept of ‘PCM-TRC slabs is interesting in many ways:

14 - The load-bearing slabs undergo heat. Therefore, the optimisation of heat transfer by PCM
15 addition has an apparent interest.

16 - The flexural behaviour of the slabs allows optimum use of the textile reinforcement.

17 **To this end, the innovative concept of a lightweight slab composed of PCM-modified**
18 **concrete reinforced with a glass textile reinforcement (PCM–TRC slab) is evaluated in**
19 **this study in terms of its mechanical behavior and thermal performance.**

20 Unlike the effect of PCMs on the mechanical behavior of ordinary concrete, few studies have
21 been conducted on the impact of PCM on the mechanical behavior of fibrous concrete and
22 TRC structures. Savija et al [30] studied the effect of PCM on the resistance of PVA fibrous
23 mortar. They observed that the addition of small amounts of microencapsulated PCM to
24 fibrous mortar can reduce its compressive strength, while having a small effect on its flexural
25 strength and deformation capacity.

26

27 Thus, the objective of this study is to **investigate the effect of PCM on the mechanical**
28 **performance of PCM–TRC slabs**, particularly their bending response. This study uses a
29 combination of mechanical tests and physicochemical investigations to explain the response
30 of the slabs to different PCM rates.

31

32 Moreover, owing to the lack of research [31, 32] on the impact of the PCM state (solid or
33 liquid) on the mechanical performance of PCM–mortar structures, this study focuses on the
34 effects of temperature (and thus PCM state) on the mechanical performances of PCM–mortar
35 matrices and their consequences on PCM–TRC slabs. The reasons for the changes in the
36 PCM–TRC slabs responses due to temperature variations are also explained.

37

38 Finally, an experimental investigation is conducted to analyse the efficiency of the PCM–TRC
39 slabs in terms of thermal performance and energy saving.

40

1 **2-Material and methods**

2 **2-1 Materials**

3 **2-1-1 Cement mortar**

4 A fine aggregate cement mortar ($D < 1.6$ mm) was used in this study to ensure the adequate
5 impregnation of the textile reinforcement for the ‘PCM-TRC’ slabs.

6 **2-1-2 PCM material**

7 The PCM used in the study was a fatty ester vegetal wax. The phase change temperature
8 ranged from 24 to 27°C with a phase change peak at 25°C. The capacity of the PCM to store
9 energy during phase change was 160 kJ/kg.

10 **2-1-3 Textile reinforcement**

11 The textile used in this study was a latex-coated AR glass fabric with a tensile resistance and
12 Young’s modulus of 800 ± 48 MPa and 53 ± 2.5 GPa respectively (informations provided by
13 the producer). The textile grid has a mesh width of 4 mm and 5 mm in the warp and weft
14 directions, respectively.

15 **2-2 Experimental methods**

16 **2-2-1 Casting procedure**

17 **2-2-1-1 Production of the PCM- mortar matrices**

18 PCM microcapsules were added at different ‘rates’ (i.e. the percentage of PCM per matrix
19 weight)

20 0, 5, 10, 15wt% to the formulation of the cement mortar. A minimum rate of 5wt% is
21 recommended to ensure a significant effect on the thermal efficiency [19].

22 Before fixing the PCM-mortar mixture compositions, a test of water absorption (table 1) after
23 24 hours of immersion in water was conducted according to EN 1097-6 [33] on the
24 hydrophilic encapsulated PCM to evaluate the amount of water absorbed by 100 grams of
25 PCM powder .

Mass of surface dried (24h in 100°C oven) PCM powder M_1 (g)	Mass of saturated PCM powder after 24h immersion M_2 (g)	Water absorption coefficient ($\frac{M_2-M_1}{M_1}$) in %
100	154	54

26 **Table 1** Test results of water absorption capacity of PCM powder
27

28 The high water demand of PCM [27, 34] is on the one hand due to its very high porosity and
29 on the other hand attributed to the existence of –OH groups on the polymer shell used for
30 microencapsulation. The -OH groups can induce chemical adsorption by creating hydrogen
31 bonds.

1 The high hydrophilic nature of PCM impairs the workability of concrete. This implies an
 2 adjustment of the $\frac{\text{total water}}{\text{cement}}$ ratio at each PCM rate to achieve equivalent conditions of
 3 impregnation of textile reinforcement in the PCM-TRC composites at each PCM rate.

4 However, it should be emphasized that since additional water in each PCM-mortar
 5 formulation is fully attributed to PCM absorption, a constant ratio of $\frac{\text{water not absorbed by PCM}}{\text{cement}}$
 6 is maintained in all the PCM-mortar formulations

7 It should also be emphasized, that a fine sand aggregate (0-1.2mm) has been chosen in the
 8 mix compositions of the PCM-mortar matrix to ensure good conditions of impregnation of the
 9 textile reinforcement which is characterized by a fine mesh opening (4mm×5mm).

10 The PCM–mortar mix compositions used for production of PCM-TRC slabs with the mortar
 11 raw materials densities are given tables 2 and 3, respectively (for 1 m³ of each formulation).

PCM-mortars	Reference		5wt% PCM-mortar		10wt% PCM-mortar		15wt% PCM-mortar	
	Mass (kg)	Volume (dm ³)	Mass (kg)	Volume (dm ³)	Mass (kg)	Volume (dm ³)	Mass (kg)	Volume (dm ³)
Cement	450	143.30	450	143.30	450	143.30	450	143.30
PCM	0	0	103.89	111.72	185.47	199.43	249.5	268.28
Fine sand (0-1.2 mm)	1668.7	632.10	1254.97	475.37	904.62	342.66	604.05	228.81
Water	216	216	261	261	306	306	351	351
Superplasticizer	9	8.60	9	8.60	9	8.60	9	8.60
Mass fraction of PCM (%)	0		5		10		15	
Volume fraction of PCM (%)	0		11.17		19.94		26.82	
$\frac{\text{Total water}}{\text{Cement}}$	0.48		0.58		0.68		0.78	
$\frac{\text{Water not absorbed by PCM}}{\text{Cement}}$	0.48		0.48		0.48		0.48	
slump (mm)	182		181		182		183	

12 **Table 2** PCM-mortar mixture compositions

Mortar components	PCM	Cement	Fine sand	Superplasticizer
-------------------	-----	--------	-----------	------------------

Real density (kg/m^3)	930	3140	2640	1046
----------------------------------	-----	------	------	------

Table 3 Real density of mortar raw materials

1

2

3 2-2-1-2 Production of the ‘PCM-TRC’ slabs

4 One-third-scale PCM–TRC slab samples ($600 \times 600 \times 45$ mm) at different PCM rates (0, 5,
5 10, 15wt%) were realised using an insitu hand lay-up technique in plywood rigid moulds
6 (**Figure 1**).

7 A suitable amount of each PCM–mortar matrix (0, 5, 10, 15wt% PCM) was spread on the
8 bottom of the mould so that 4 mm cover layer was applied between the bottom textile
9 reinforcement layer and the lower slab face. Then, the reinforcement was impregnated by the
10 matrix with a roller such that the matrix penetrated the textile fabric meshes. The procedure
11 was repeated so that the PCM–TRC slabs were reinforced with a textile layer every 5 mm
12 thick in the in-tension area of the slab (the volumetric rate of reinforcement was 4.78%).

13 The slabs were tested using three-point bending. Special attention was given to the placement
14 of the AR glass reinforcement in the area subjected to tensile stresses (the textile
15 reinforcement was placed in the lower half of the slabs under the neutral axis).

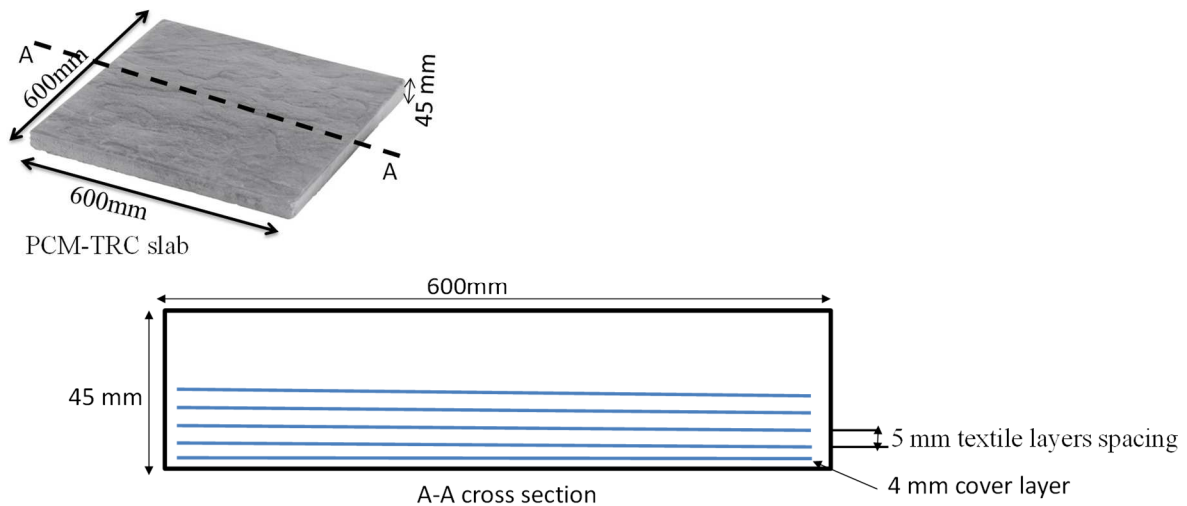


Textile placement

Textile impregnation

A- Insitu hand lay-up technique

16



B- PCM-TRC slab A-A cross section with the textile reinforcement

Figure 1 A- Insitu hand lay-up technique, B-PCM-TRC cross section

1
2

3 2-2-2 Mechanical characterisation

4 2-2-2-1 Matrix scale

5 2-2-2-1-1 Mechanical behavior of PCM–mortar matrix at different PCM rates and
6 temperature conditions

7 Compression and bending tests were conducted on specimens containing 0, 5, 10, and 15wt%
8 PCM with a loading speed of 2.4 kN/s for compression test and 0.015 mm/s for bending test
9 according to EN 196-1[35] by considering two specimen temperatures: ambient temperature
10 (maximum of 20°C) and a temperature of approximately 40°C. Five samples for each PCM
11 rate and temperature condition were tested.

12 The samples tested at 40°C were placed for 6 h in an oven to induce a PCM phase change
13 from solid to liquid. The tests were conducted 3 min after the samples were removed from the
14 oven (five samples were tested for each PCM rate) to preserve the temperature homogeneity
15 in the test samples.

16 A temperature of 40°C was chosen to be sufficiently high to ensure complete melting of the
17 PCM and to limit the risk of temperature drop, which could lead to tests with the PCM in the
18 liquid-to-solid transition phase. This temperature was also sufficiently low to ensure that the
19 assumption of the absence of damage to the PCMs or mortar due to temperature before the
20 tests was true. The age of the samples during testing was 28 days.

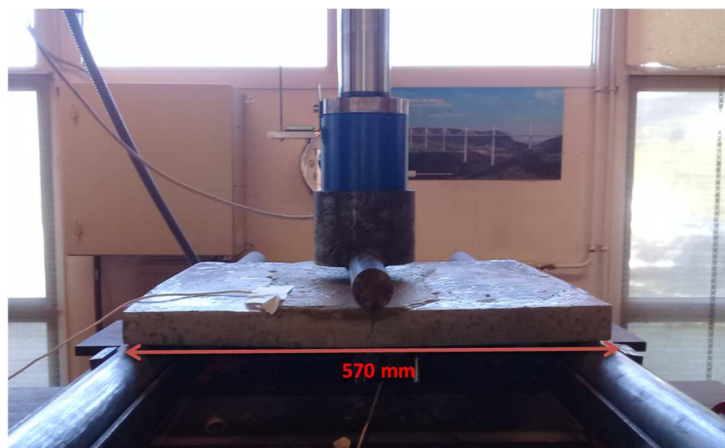
21 Five additional samples (of each PCM rate) were heated at 40°C then cooled to 20°C for 6 h
22 in a temperature-conditioned room to allow homogeneous resolidification of the PCM. The
23 tests on the heated then cooled samples were conducted 3 min after removing them from the
24 temperature-conditioned room.

1 2-2-2-2 Structural element scale ('PCM-TRC' slabs)

2 2-2-2-2-1 Efficiency of textile reinforcement

3 To verify the effectiveness of textile reinforcement, three-point bending tests (**Figure 3**) with
4 a loading speed of 0.2 mm/min, over a span of 570 mm, were conducted on a 600 × 400 × 45
5 mm unreinforced control slab without PCM and on a textile-reinforced slab without PCM
6 (with a textile reinforcement rate of 4.78% in the in-tension zone). Three samples per
7 specimen configuration were evaluated.

8



9

10

Figure 3 Three points bending test on PCM-TRC slab

11

12 2-2-2-2-2 Mechanical tests at variable PCM rate and constant temperature

13 PCM-TRC slabs (600×400×45mm) at different PCM rates (0, 5, 10 and 15wt%) were tested
14 in displacement imposed three points bending with a loading speed of 0.2 mm/min and over a
15 span of 570 mm

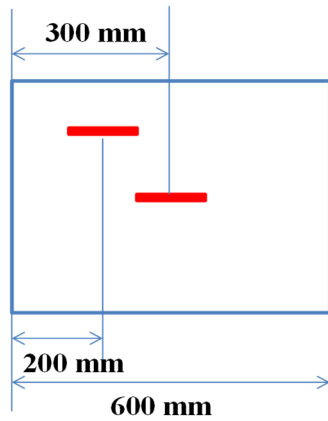
16 The temperature during the tests was maintained at 20°C (the PCM incorporated in the slabs
17 is therefore in the solid state).

18 Three slabs per PCM rate were tested during this experimental campaign to ensure the
19 reproducibility of the results.

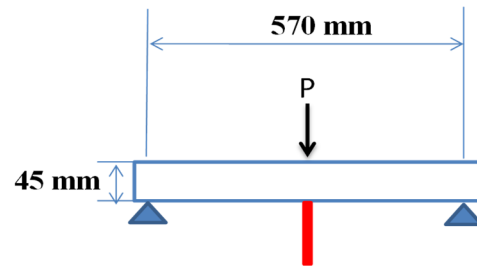
20 The instrumentation used for the tests (**Figure 4**) comprised

21 1-An LVDT sensor vertically positioned at mid-span to measure the deflection of the slabs
22 during the test.

23 2-Two LVDT sensors in a horizontal position to measure the elongation of the slabs in the in-
24 tension face, over a measurement length of 200 mm. The first LVDT sensor was placed in the
25 central zone of the in-tension face, and the second sensor was offset by 30 cm from the first.



Bottom view of the instrumentation face of the slab



Front view of the slab

Legend :  LVDT sensor placement

1

2

Figure 4 Instrumentation of bending tests on PCM-TRC slabs

3

2-2-2-2-3 Mechanical tests at variable temperature and constant PCM rate

4

The 10wt% PCM-TRC slabs with the same reinforcement rate (4.78%) underwent three-point bending tests under different temperature conditions to evaluate the effect of the PCM state on the mechanical performance of the PCM-TRC slabs (at the structural element scale). 10wt% PCM-TRC slabs at different temperatures were evaluated as described below:

5

6

7

8

A- A slab was maintained at 20°C and then underwent three-point bending tests at the same temperature

9

10

B- A slab was heated to 40°C for 6 h and then tested 3 min after being removed from the oven.

11

12

For sake of completeness, all the described tests section 2-2-2 are summarized **Table 4**

13

14

15

16

17

18

19

20

21

22

23

24

25

26

1

Type of test	Number of identical samples	Examined parameters
PCM-mortar compression and bending tests	5	- Strength at different temperatures - Rate of strength decrease due to PCM rate - Rate of strength decrease due to temperature - Rate of strength recovery due to temperature
PCM-TRC slabs bending tests at constant temperature and different PCM rates	3	- Force at failure - Force at first crack - Deflection at failure - Textile exploitation ratio - Average crack spacing
PCM-TRC slabs bending tests at constant PCM rate and different temperatures	2	- Force at failure - Force at first crack - Deflection at failure - Average crack spacing

2 **Table 4** Summary of the examined parameters during the tests described section 2-2-2

3 2-2-3 SEM observations

4 To have a better understanding of the impact of PCM on the mechanical behavior of PCM-
5 TRC slabs, SEM observations (on a MIRA FEG SEM) were conducted at the matrix/textile
6 scale on a few samples of PCM-TRC composites at different PCM rates (the samples were
7 realised beforehand for SEM observations). A backscattered electron detector was used to
8 identify the different phases existing at the matrix/textile interface scale.

9 All the examined parameters are also summarized **Table 5**

Type of test	Number of identical samples	Examined parameters
SEM observation on PCM-TRC samples at matrix/textile interface	2	- Pore sizes at the matrix/textile interface - Matrix/textile interaction - Chemical characterisation (EDS analysis) at the matrix/textile interface

10 **Table 5** Summary of the examined parameters during the SEM observation

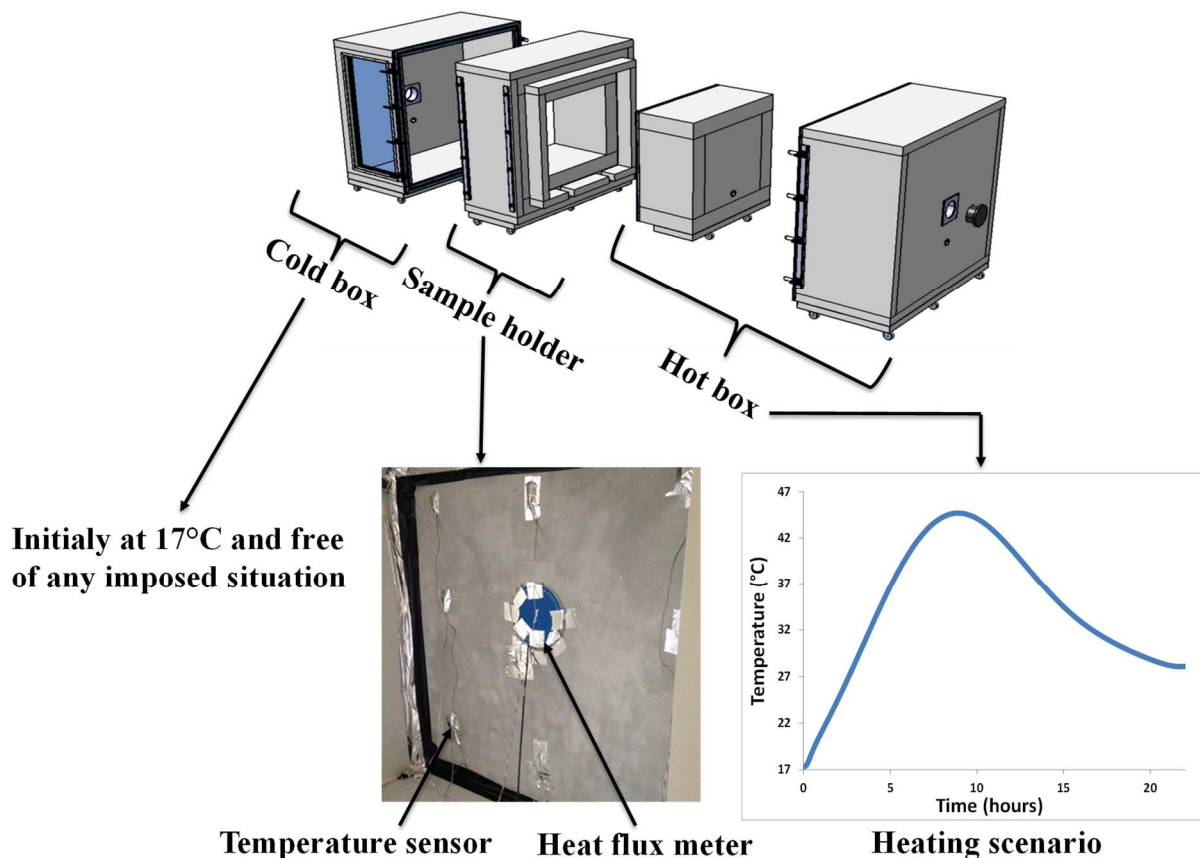
11 2-2-4 Thermal performance evaluation

12 The thermal inertia of 1010 × 1010 × 45 mm PCM-TRC slabs was evaluated using a guarded
13 hot box. The instrumentation during the test follows the recommendations of the standard
14 ASTM C 236[36]. The guarded hot box comprised a hot-side enclosure, cold-side enclosure,

1 and sample holder between the two enclosures where the test sample was placed (**Figure 5**).
2 The same slab thickness used during the mechanical tests was considered for the thermal
3 inertia test.

4 To evaluate the thermal inertia of the PCM–TRC slabs, similar scenarios were imposed on the
5 reference slab (without PCM) and 10wt% PCM–TRC slab (slab with 10wt% PCM rate). The
6 scenarios were as follows: first, the temperature was increased from 17 to 45 °C in 8 h on the
7 hot side of the guarded hot box; second, the heating resistances in the hot chamber were
8 turned off. The cold side remained free of any imposed stress throughout the entire scenario
9 (see the imposed scenario **in Figure 5**). The aim was to analyse the effect of PCM addition on
10 the air temperature and surface temperature of the slabs on the cold side. The imposed
11 scenario corresponds to a situation wherein the hot side represents the outside temperature and
12 the cold side represents the feeling inside a home.

13 Temperature sensors with a resolution of 0.1°C were positioned on the surfaces of the PCM–
14 TRC slabs on the hot and cold sides of the samples. Two air temperature sensors were also
15 positioned in each enclosure (on the hot and cold sides). The heat flux was measured thanks
16 to the heat flux meters placed in the surface of the slabs in the two sides (in the hot and cold
17 side of the guarded hot box).
18



19 **Figure 5** Imposed scenario in the guarded hot box for thermal inertia test on ‘PCM-TRC’
20 slabs
21
22

1

2

3 All the examined parameters during the test are summarized **Table 6**

Type of test	Number of identical simples	Examined parameters
Thermal inertia of PCM-TRC slabs	1	<ul style="list-style-type: none"> - Sample surface temperature in hot box - Air temperature in the hot box - Sample temperature in the cold box - Air temperature in the cold box - Heat flux in the hot and cold box - Stored energy by the sample

4

Table 6 Summary of the examined parameters during the thermal inertia test

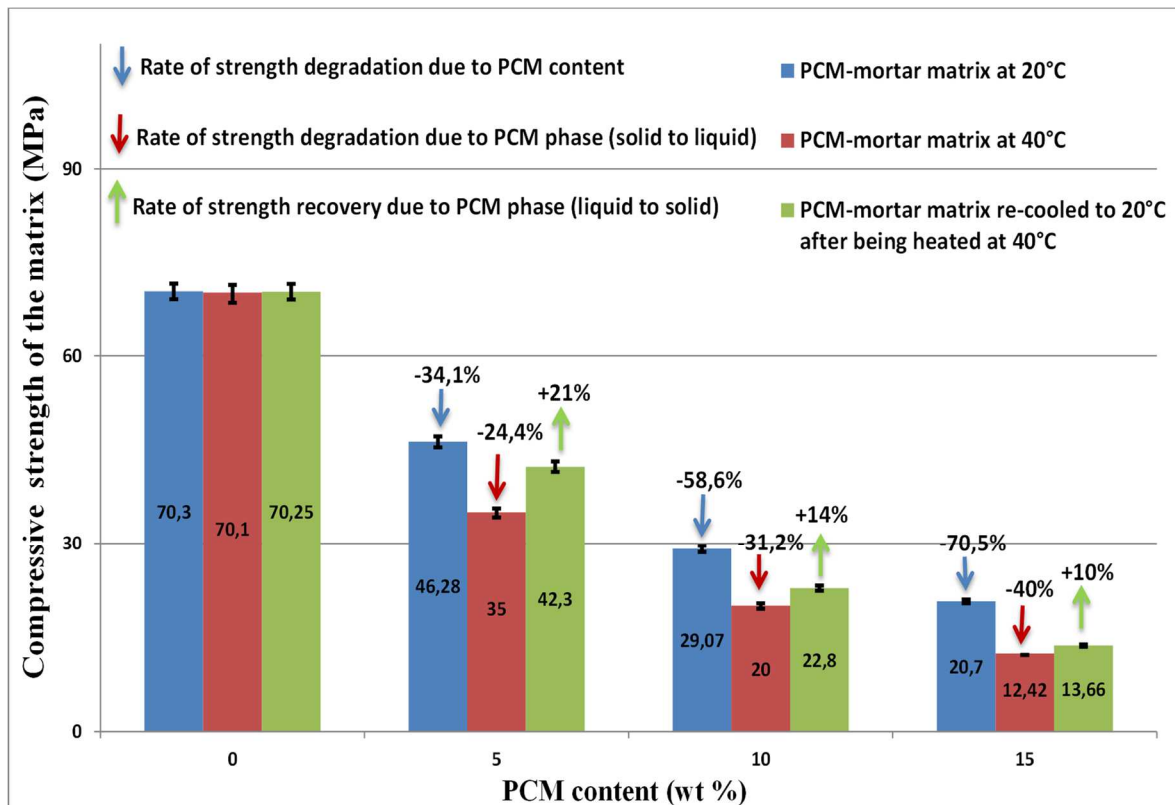
5 **3-Results and discussion**

6 3-1 Mechanical characterisation

7 3-1-1 Matrix scale

8 3-1-1-1 Mechanical characterisation of PCM-mortar matrices

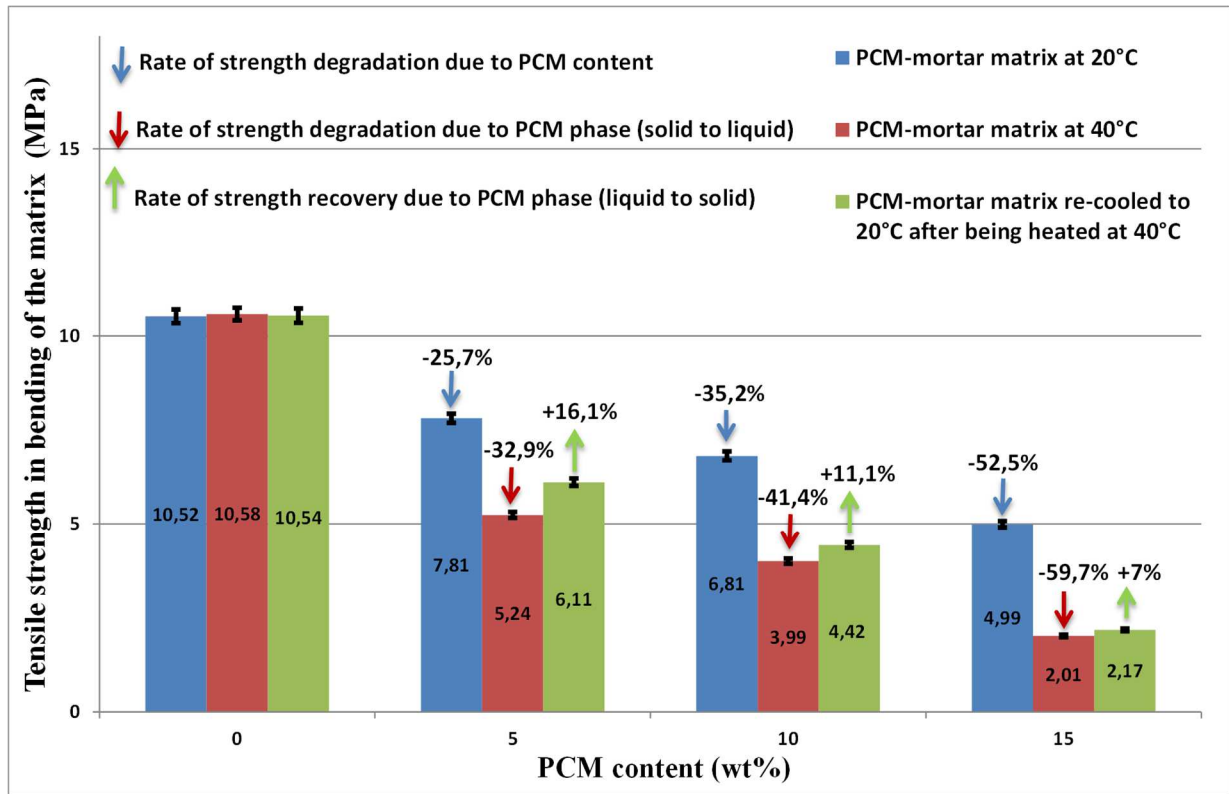
9 **Figure 6** depicts compressive and tensile strength in bending of the 28-day matrices with
 10 different PCM rates. The tests were conducted under three temperature conditions: samples
 11 whose temperature was maintained at 20°C, samples heated to 40°C, and samples cooled to
 12 20°C after heating at 40°C.



13

1
2

(a)



3
4

(b)

Figure 6 Effect of PCM rate and state on (a) the compressive strength (b) tensile strength in bending of PCM-mortar matrix

7

The main results derived from the experimental tests presented above are as follows:

8
9
10

(a)-The resistance of the PCM–mortar matrices decreased as the PCM rates increased during the mechanical tests of compression and bending. This observation was valid regardless of the temperatures.

11
12
13

(b) Significant degradation in the mechanical performance of the PCM–mortar matrices was observed when the PCM changed from the solid to liquid state after heating. The rate of strength deterioration increases when increasing PCM content in the matrices.

14
15
16

(c) Mechanical tests conducted on the PCM–mortar matrices cooled to 20°C after heating at 40°C for 6 h indicated that the initial strengths of the PCM–mortar samples were only partially restored.

17
18
19
20
21

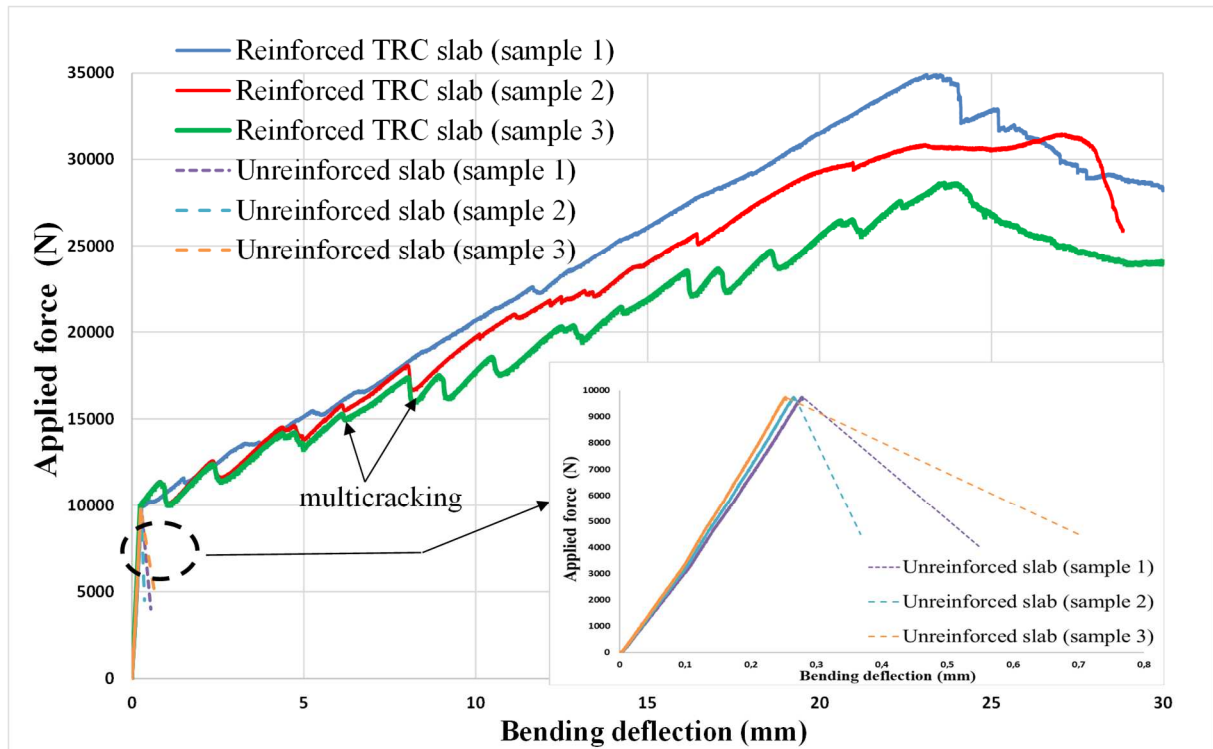
Observations (b) and (c) can be attributed to the phenomenon of PCM expansion during phase change observed by the authors in [26, 33]. The transition from the solid to liquid state induces an increase in the PCM microcapsule volume, which can induce microcracking in the matrix (i.e. local strains). These microcracks are responsible for the degradation of the mechanical performance of the matrices and the partial restoration of the initial properties.

22

3-1-2 Structural element scale ‘PCM-TRC slabs’

1 3-1-2-1 Efficiency of the textile reinforcement

2 The results of the three-point bending tests in terms of (force vs deflection) on unreinforced
3 reference slabs (without PCM) and on reference slabs with a 4.78% rate of textile
4 reinforcement in the in-tension area are depicted in **Figure 7**.



5 **Figure 7** Three-point bending test result on reinforced and unreinforced slabs

6
7
8 The unreinforced slabs exhibited brittle behavior where the failure occurred directly after
9 reaching the ultimate tensile stress of the mortar. A single macrocrack at mid-span followed
10 by the simultaneous failure of the slab was observed (**Figure 8**).

11 In the reinforced slabs, a ductile and multicracking behavior was observed (see **Figure 8**,
12 which depicts the cracking pattern in the in-tension area of the slab), synonymous to a
13 matrix/textile stress transfer during the test. Failure of the reinforced slab occurred by
14 compression crushing in the compressed face at mid-span.

15 Two distinct phases can be clearly identified in the reinforced slab (**Figure 7**). The first phase
16 (**phase I, Figure 7**) corresponds to the elastic behavior of the slab. This phase ends at the
17 occurrence of the first crack. The second phase (**phase II, Figure 7**) is associated with the
18 change in slope on the force–deflection curve. This phase corresponds to the redistribution of
19 forces from the cracked matrix towards the textile reinforcement at each crack in the in-
20 tension area of the slab.

21



Brittle behaviour of unreinforced TRC slab



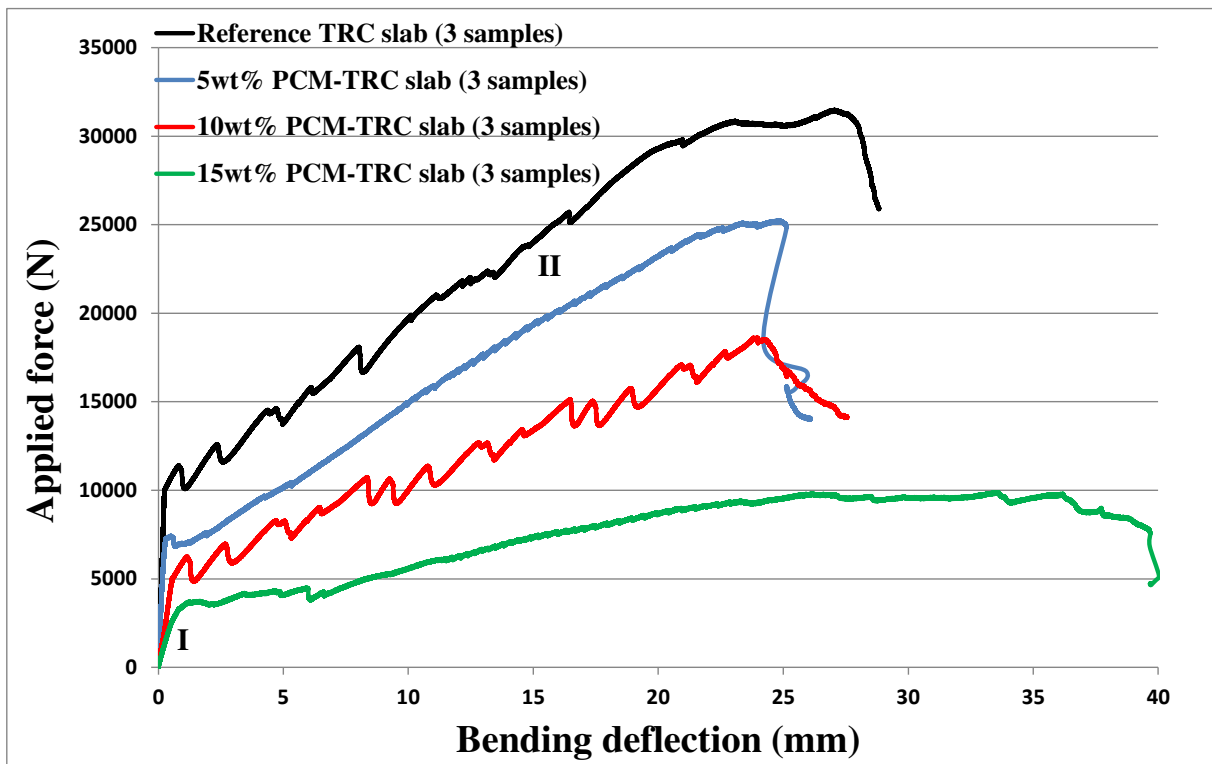
Ductile and multicracking behaviour of reinforced TRC slab

1
2 **Figure 8** Behavior of reinforced and unreinforced slabs

3 3-1-2-2 Mechanical tests at variable PCM rate and constant temperature

4 3-1-2-2-1 Global behavior

5 The results of the three-point bending tests in terms of (force vs deflection) at a constant
6 temperature of 20°C on the 0, 5, 10, and 15wt% PCM–TRC slabs are depicted in **Figure 9** (all
7 experimentally derived curves for three samples per each PCM-TRC configuration are also
8 presented **Appendix 1** at the end of the manuscript). The main characteristics of the PCM–
9 TRC slabs during the three-point bending tests are summarised in **Table 7**.



10
11 **Figure 9** Bending test results on PCM-TRC slabs at different PCM rates (constant
12 temperature)

13

PCM-TRC slabs	Unreinforced slab	Reference TRC slab	5wt% PCM-TRC slab	10wt% PCM-TRC slab	15wt% PCM-TRC slab
Force at first crack (kN)	9.8±0.4	9.76±0.4	7.2±0.3	4.7±0.2	2.9±0.12
Force at failure (kN)	9.8±0.4	31.6±1.9	25±1.7	19.7±1.2	9.9±0.5
Deflection at failure (mm)	0.4±0.1	23.9±0.8	23.3±0.7	23.9±0.7	36.1±2.8
Textile exploitation ratio (%)	/	82.12±3.5	72.98±3.0	48.38±2.3	27.88±1.9
Average crack spacing (cm)	/	2.0±0.1	2.65±0.1	3.7±0.1	5.1±0.1

2

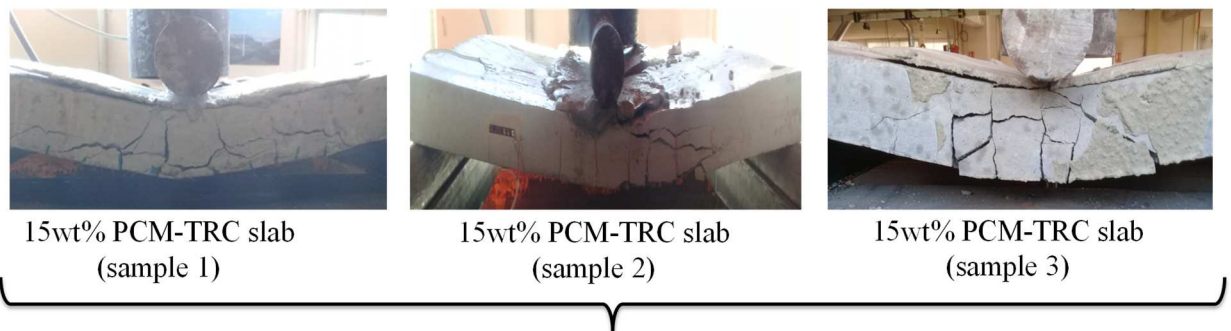
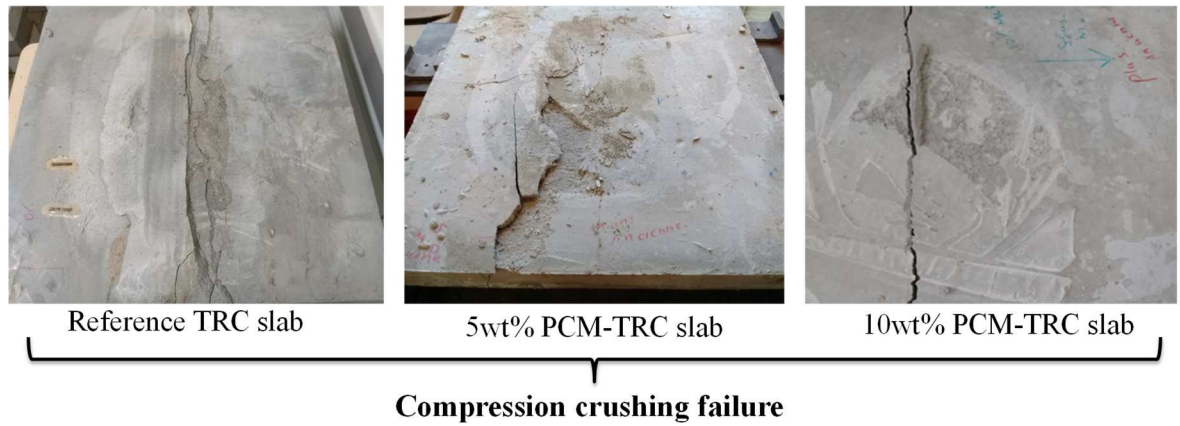
Table 7 Performance characteristics of PCM-TRC slabs during bending test

3 From the results presented in **Figure 9** and **Table 7**, it can be seen that the load-bearing
4 capacity of the slabs decreases with the increase in the PCM rate.

5 By analysing the force–deflection curves in detail, it can be deduced that

6 - The elastic phase I (phase I in **Figure 9**) is characterised by a degradation in the mechanical
7 performance (force at first crack and bending rigidity) of the PCM–TRC slabs with the
8 increase in the PCM rate, in accordance with **Section 3-1-1**. In fact, the mechanical
9 performance of the slabs in phase I is mainly dependent on the mechanical performance of the
10 PCM–mortar matrices, which is degraded by the increasing amount of PCM.

11 - In the textile contribution phase II (phase II in **Figure 9**, which begins at the occurrence of
12 the first crack and ends at failure), the load is transmitted progressively from the matrix to the
13 textile reinforcement at the occurrence of each crack. It can be observed that the 0, 5, and 10
14 wt% PCM–TRC slabs exhibit almost identical deflections at failure, **whereas the 15wt%**
15 **PCM–TRC slab** exhibits a greater deflection. This is explained by the particular mode of
16 failure of the latter. In fact, the mode of rupture of the 15wt% PCM-TRC slab is due to
17 inferior matrix-to-textile bond conditions that induced textile slippage from the matrix leading
18 to larger deflections and a deeper compression zone (**Figure 10**). Conversely, the failure
19 modes of the 0, 5, and 10wt% PCM–TRC slabs occur due to a sudden compression crushing
20 of the matrix (**Figure 10**).

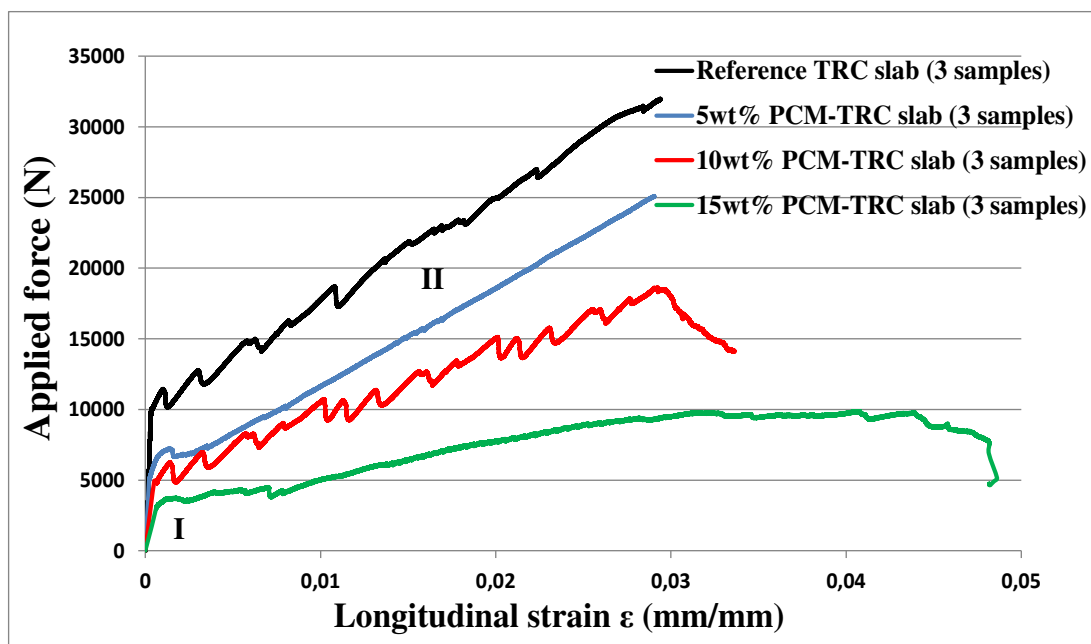


1 **Failure due to textile slippage induced by poor bond conditions for 15wt% PMC-TRC slabs**

2 **Figure 10** Failure modes of PCM-TRC slabs in bending tests at constant temperature

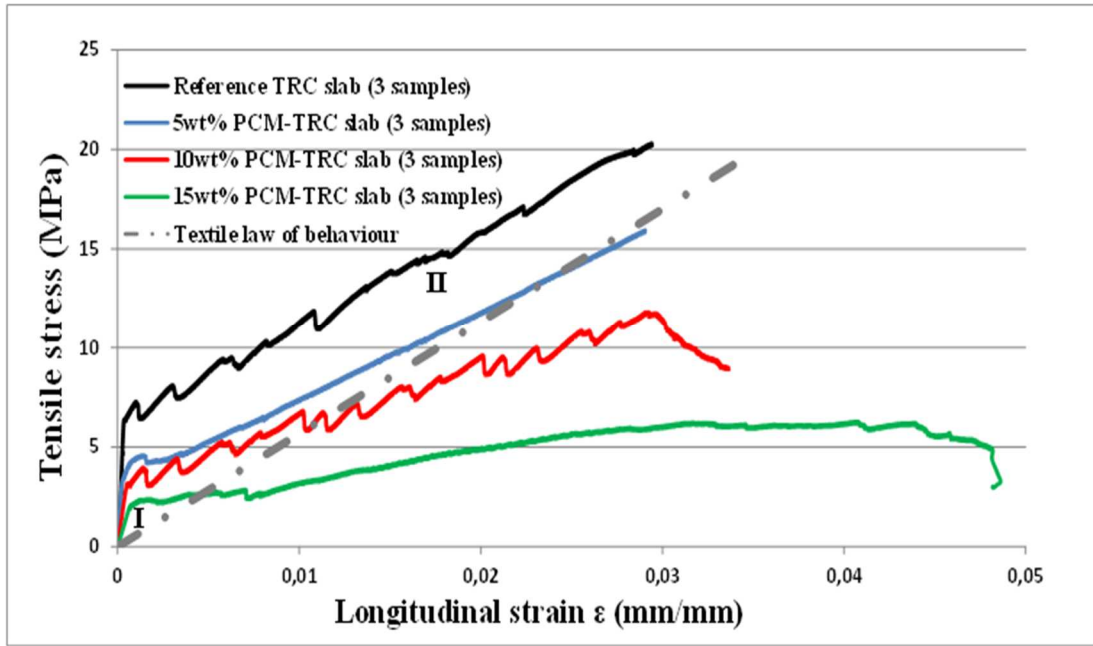
3 3-1-2-2-2 Local behaviour (LVDT sensors and crack spacing)

4 The graph of the (force vs longitudinal axial strain) and (Tensile stress in the in-tension part
 5 of the section of the slabs vs longitudinal strain) in the mid-span area is illustrated in **Figure**
 6 **11** (obtained by the LVDT sensor placed in the central zone of the in-tension face, **Section 2-**
 7 **2-2-2-2**).



(a)

1



(b)

2
3

4 **Figure 11** (a) Force vs longitudinal strain at mid-span (b) Tensile stress in the in-tension part
5 of the section at mid-span

6 The curves are divided into two phases:

7 **Phase I** with high rigidity corresponding to the evolution of the strain of the uncracked matrix

8 **Phase II** is characterised by a significantly lower rigidity corresponding to the strain
9 evolution of the in-tension face during the phase of matrix multicracking and the
10 matrix/textile load transfer at the occurrence of each crack. For the 15 wt% PCM, a higher
11 strain at failure was observed, which can be explained by inferior matrix-to-textile bond
12 conditions that induced textile slippage from the matrix (**Figure 10**). The LVDT sensors
13 positioned in the in-tension face of the 15 wt% PCM-TRC slab measured the slip
14 displacement of the interlaminar layer upon the occurrence of textile slippage, which explains
15 the higher strain at failure for the 15 wt% PCM-TRC slab in comparison with those of the 0,
16 5, and 10 wt.% PCM-TRC slabs.

17 The textile slippage failure mode of the 15wt% PCM-TRC slab observed at the structural
18 element scale is also consistent with the textile slippage rupture observed at the composite
19 material scale in the tensile tests conducted by the authors [24, 32] on PCM-TRC composite
20 samples at a PCM rate of 15wt%.

21 **Figure 12** presents the textile exploitation ratio (textile work ratio) defined by the ratio $\frac{E_{II}}{E_{Textile}}$
22 (E_{II} represents the slop of the tensile stress vs strain in the phase II of figure 11-b , $E_{Textile}$
23 represents the textile modulus taking into consideration the textile volume ratio)

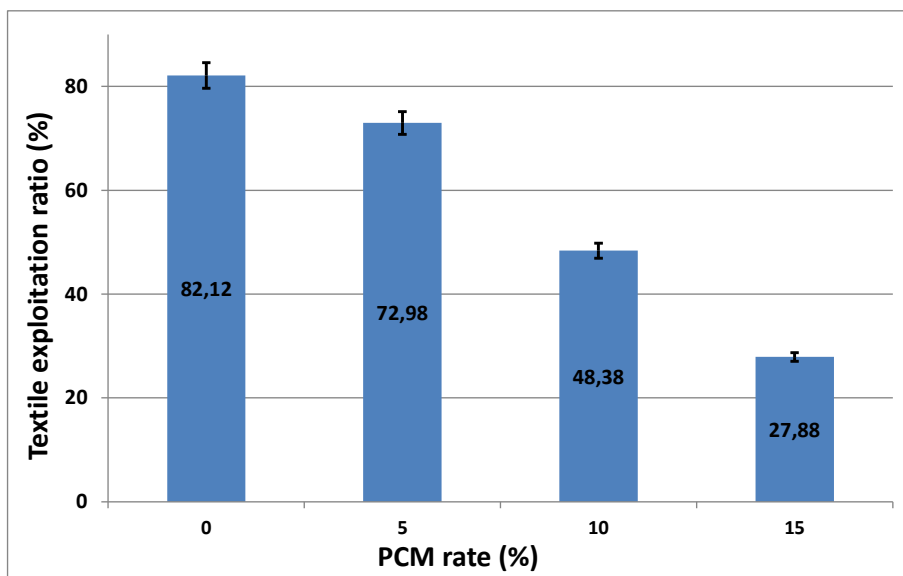


Figure 12 Evolution of the textile exploitation ratio with PCM rate

The textile exploitation ratio (textile work ratio) decreases with the PCM rate. This indicates a degradation in the intensity of the ‘matrix/textile’ interaction with the increase in the PCM content (degradation of the textile effectiveness).

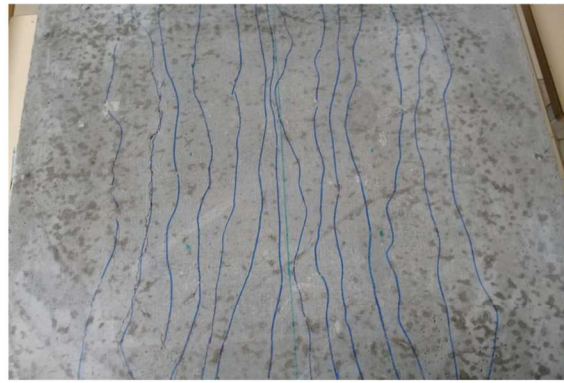
It can also be seen from **Table 7 and Figure 13** that the average spacing between two consecutive cracks increases with the increase in the PCM rate. In other words, the total number of cracks decreases with the PCM content in the PCM–TRC slabs.

The average spacing between two consecutive cracks is directly related to the intensity of the matrix/textile interaction (more precisely, the matrix/textile contact surface area) as the appearance of a crack is synonymous to a matrix/textile stress transfer in the zone of crack apparition. Consequently, the matrix/textile stress transfer behavior increase with the increase in the number of cracks.

According to the crack spacing results (**Table 7 and Figure 13**), augmenting the PCM rate has a negative effect on the matrix/textile load transfer behavior. This confirms the analysis of the slope of the tensile stress–longitudinal strain curves in phase II in **Figure 11-b**. More clarifications on the effect of PCM on matrix/textile stress transfer behavior are provided in **Section 3-2**.



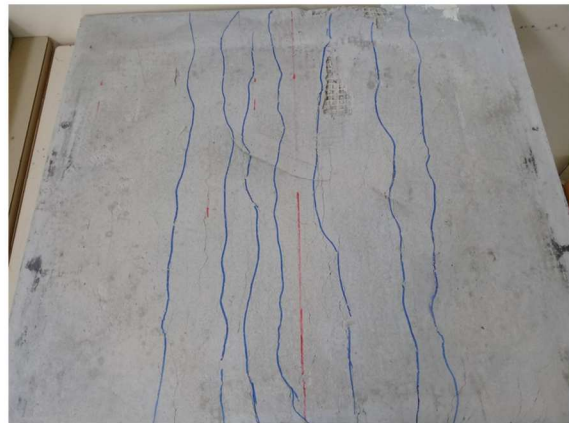
Reference PCM-TRC (2,0 cm crack spacing)



5wt% PCM-TRC (2,65 cm crack spacing)



10wt% PCM-TRC (3,70 cm crack spacing)



15wt% PCM-TRC (5,10 cm crack spacing)

Figure 13 Average crack spacing in the in-tension face for PCM-TRC slabs

1
2
3

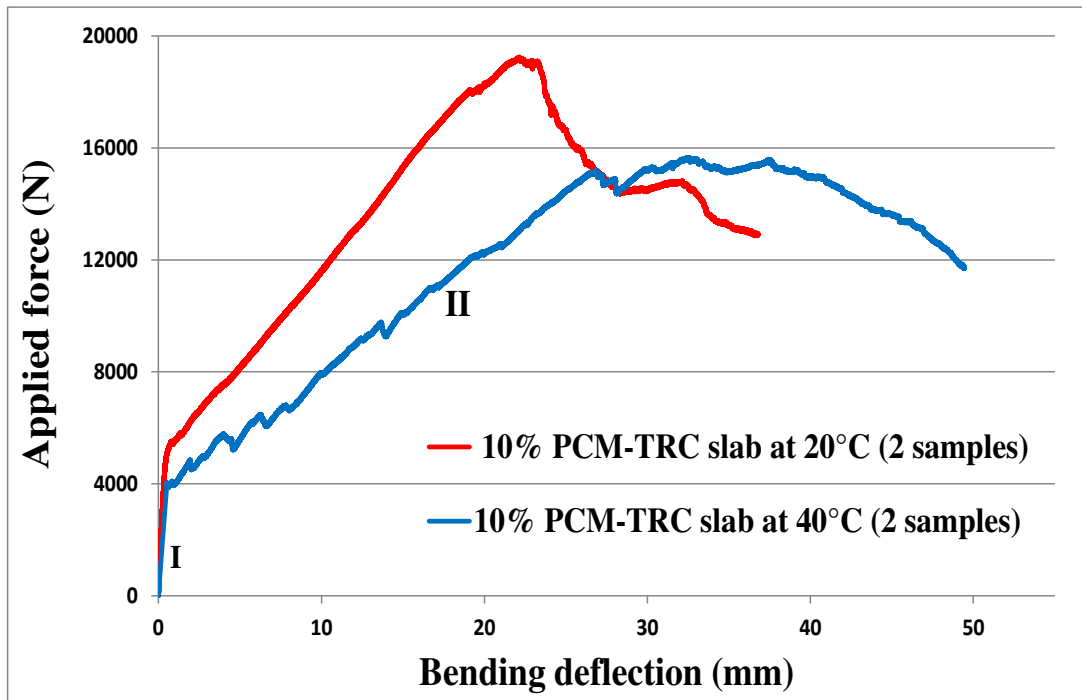
4 3-1-2-3 Mechanical tests at variable temperature and constant PCM rate

5 Bending tests were conducted on 10wt% PCM-TRC slabs conserved at temperatures of 20
6 and 40°C, respectively.

7 The 10wt% PCM-TRC slab was selected for this test because it presents an optimum balance
8 between its mechanical properties and thermal performance.

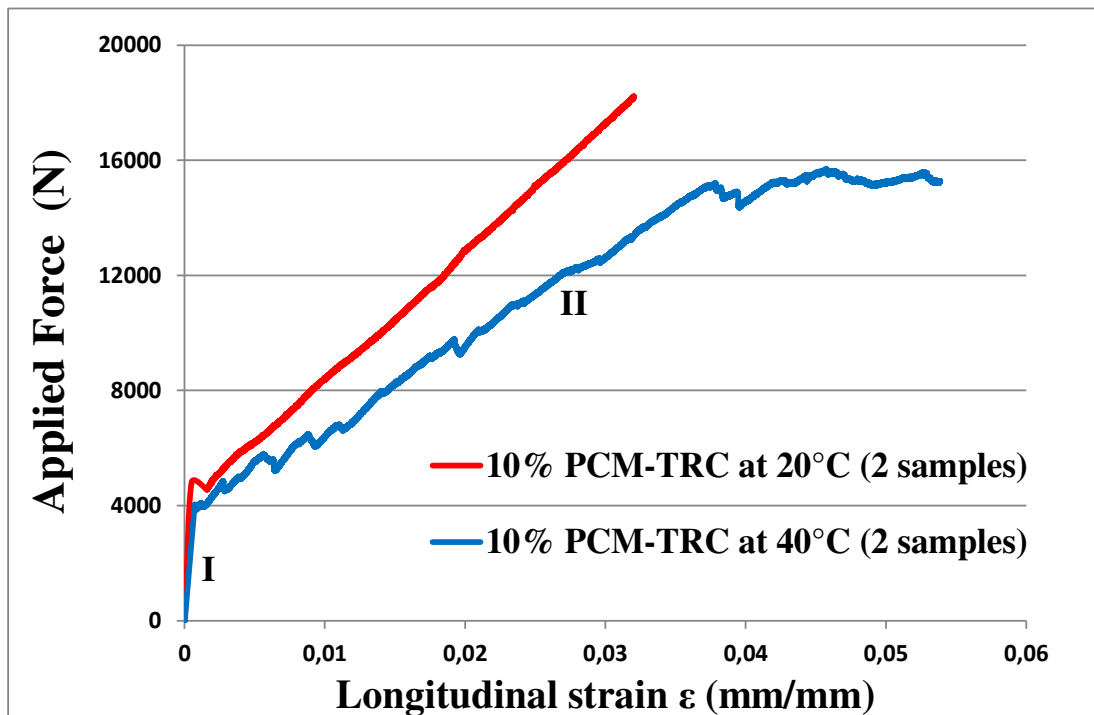
9 The results of the three-point bending tests in terms of (force vs deflection at mid-span and
10 force vs axial deformation in the in-tension face at the mid-span area) on 10wt% PCM-TRC
11 slabs maintained at 20°C and heated to 40°C are depicted in **Figures 14-a and 14-b.**

12



1
2

-a-



3
4

-b-

5 **Figure 14** Effect of temperature on -a- force vs deflection and -b- force vs strain (central
6 zone)

7 The results depicted in **Figures 14-a and 14-b** indicate a slight decrease in the force at the
8 appearance of the first crack (elastic phase), as well as a degradation of the load-bearing
9 capacity of 21% for the 10wt% PCM-TRC slab heated to 40°C with respect to the slab
10 maintained at 20°C. In addition, the failure mode of the slab heated to 40°C occurred by
11 textile slippage initiated at the interlaminar space between the two lower textile reinforcement

1 layers (**Figure 15**) at a force of 15000 N, whereas the failure mode of 10% PCM–TRC slabs
2 maintained at 20°C occurred by compression crushing (**Figure 15**).

3 The textile slippage was confirmed by analysing the evolution of the longitudinal strain of the
4 in-tension face at mid-span (**Figure 14-b**), wherein at a force of 15000 N, an increase in the
5 strain is observed at an almost constant force for 10wt% PCM-TRC slab heated at 40°C. The
6 measured strain during the delamination is due to the textile slippage caused by the
7 degradation of the shear strength of the interlaminar layer (the layer between two textiles
8 reinforcements) when PCM was at 40°C (the LVDT sensor placed in the in-tension face
9 measures a parasitic deformation attributed to textile slippage).

10 A more detailed analysis of **Figure 14-b** also reveals a 30% decrease in the slope of the curve
11 (force vs strain of the in-tension face at mid-span) in **phase II** for the 10wt% PCM–TRC slab
12 heated at 40°C. This slope is directly proportional to textile reinforcement work ratio. The
13 increase in the average crack spacing between two consecutive cracks in the in-tension faces
14 for the slab heated at 40°C (average crack spacings of 3.6 cm and 4.3 cm for the 10wt%
15 PCM–TRC slabs maintained at 20°C and heated at 40°C, respectively) confirms the
16 deterioration of the matrix/textile interaction due to the effect of PCM state.

17 The degradation of the matrix/textile stress transfer (decrease in the textile work ratio ‘textile
18 efficiency ratio’ in terms of stiffness) in addition to the weakening of the shear strength of the
19 interlaminar layer (rupture by textile slippage) for the 10% PCM–TRC slab heated to 40 °C
20 are most likely attributed to the effect of microcracking due to PCM expansion during its
21 phase change. The microcracks at the matrix/textile interface can disturb the stress transfer
22 from the matrix to the cracked interface until the textile reinforcement.



Compression crushing failure
10wt% PCM-TRC slab at 20°C



Delamination failure
10wt% PCM-TRC slab at 40°C

23
24 **Figure 15** failure modes of 10wt% PCM-TRC slabs at different temperatures

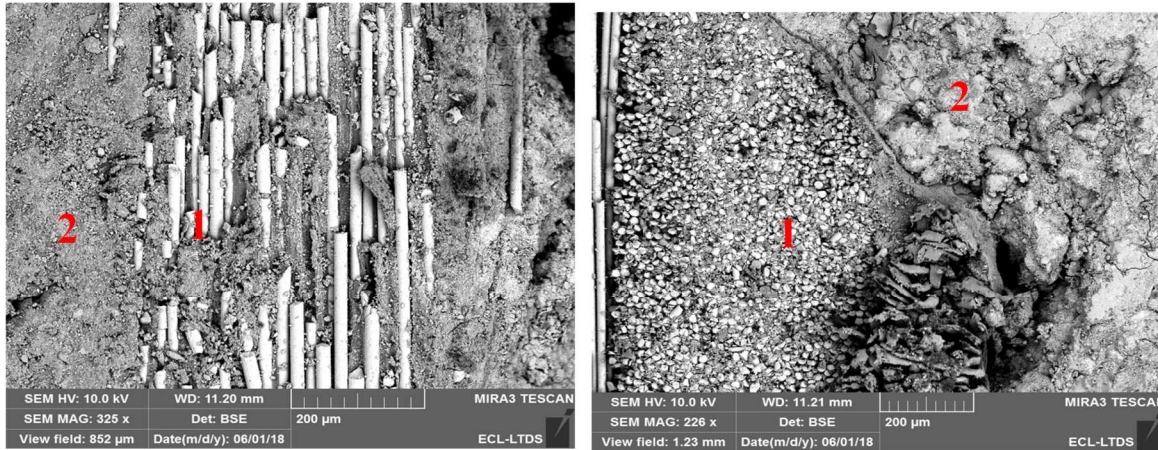
25 3-2 SEM observations

26 It has been demonstrated in the previous sections that the addition of PCM induces
27 mechanical performance degradation of the PCM–TRC slabs. The following SEM

1 observations help further explain the effect of PCM on stress transfer at the matrix/textile
2 interface.

3 3-2-1 SEM observation in a reference 'PCM-TRC' composite (without PCM)

4 **Figure 16** depicts the SEM observation of longitudinal and transversal cross-sections at the
5 matrix/textile interface in a reference TRC composite (without PCM).



A- Longitudinal cross section

B- Transversal cross section

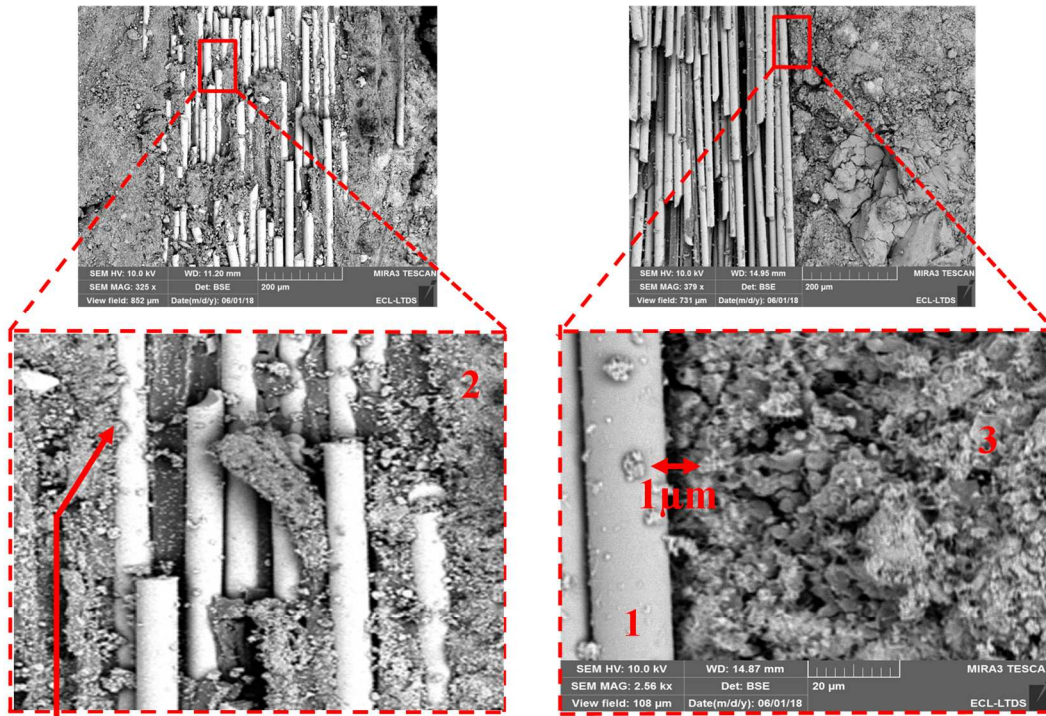
Legend: 1 Fiber yarn impregnated with latex, 2 matrix without PCM

6

7

Figure 16 SEM image of the reference TRC composite (without PCM)

8 A high degree of matrix/textile interaction can be observed. There is less porosity at the
9 interface transition zone (ITZ) between the matrix and the fabric in the reference TRC
10 (without PCM) compared to PCM-TRC composites (with the addition of PCM). In fact, SEM
11 observation allows quantifying an ITZ spacing of 30 to 50 nm in the case of reference TRC
12 composite while it varies between 1μm and 2 μm in function of the PCM rate in PCM-TRC
13 composites (**Figure 17**). This explains the high textile work ratio and the lowest average crack
14 spacing observed for the reference TRC slab.



High interaction

Reference TRC

10wt% PCM-TRC

Legend: 1 Textile yarn, 2 matrix without PCM, 3 matrix with PCM inclusion

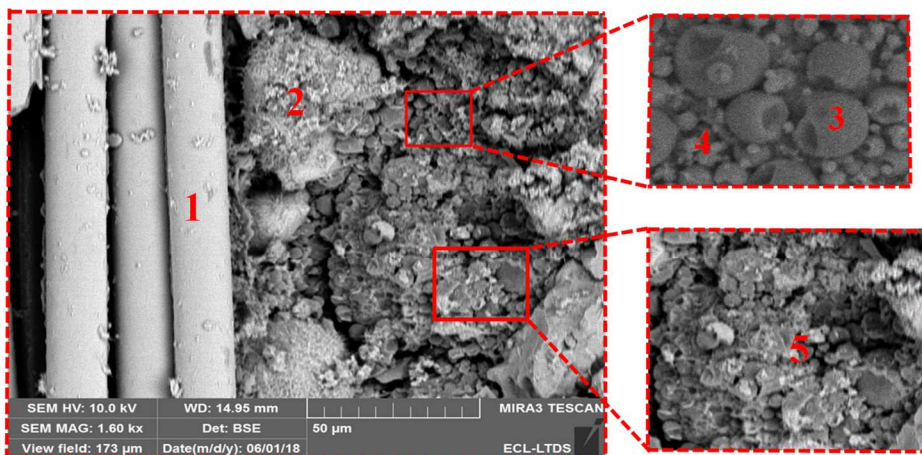
1
2

Figure 17 effect of PCM on ITZ ‘matrix/textile’ in PCM-TRC composites

3 3-2-2 SEM observations in the PCM-TRC composites (with PCM inclusions)

4 3-2-2-1 Effect of PCM on cement hydration in the proximity of the interface

5 **Figure 18** depicts an SEM image of a 15wt% PCM–TRC composite that illustrates the
6 consequences of the effect of PCM on the matrix hydration in the proximity of the
7 matrix/textile interface.



Legend : 1 Textile, 2 Cement, 3 PCM microcapsule, 4 nodules of pure PCM wax, 5 Agglomeration of PCM

8
9

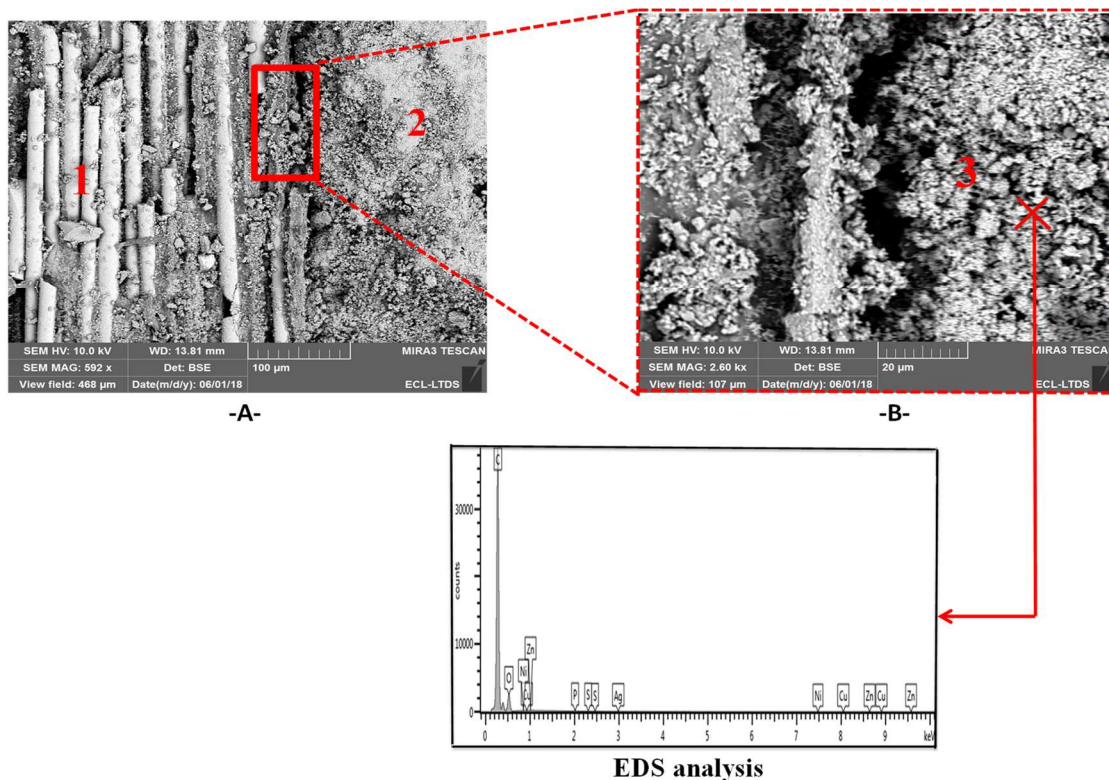
Figure 18 SEM image illustrating the effect of PCM on cement hydration near the interface

1 From **Figure 18**, it can be observed that the chain of PCM capsules (**legend 3**) that surround
2 the anhydrous cement (**legend 2**) in the immediate vicinity of the matrix/textile interface can
3 inhibit its hydration by restricting its access to water, thereby reducing the amount of hydrated
4 products from the cement in the interface zone. The consequence is a loss of the matrix/textile
5 bond and a reduction of the textile exploitation ratio.

6 At the local scale of PCM, SEM observation also reveals that some damage may occur to the
7 PCM microcapsules (**legend 3 in Figure 18**) inducing the leakage of pure PCM in the form of
8 micronodules (**legend 4 in Figure 18**).

9 3-2-2-2 Effect of PCM leakage at the interface proximity

10 **Figure 19** depicts another SEM observation of the 15wt% PCM–TRC composite, which
11 demonstrates the effect of the deposition of large quantities of pure PCM wax (leaked from
12 PCM capsules) in the immediate vicinity of the matrix/textile interface. The deposition of
13 these quantities is illustrated in the framed area of **Figure 19** and confirmed by the EDS
14 analysis that indicates the presence of an intense peak of carbon with a less pronounced peak
15 of oxygen that are high probably attributed to pure PCM oil ($\text{CH}_3\text{-CH}_2(14)\text{-C(O)-O-CH}_2$).
16 These quantities are most likely attributed to the damage of PCM microcapsules during the
17 manufacture of the PCM–TRC composite using the hand lay-up technique. The progression of
18 the CSH hydrate growth (**CSH gel is visible in legend 2 of Figure 19**) is inhibited in the
19 deposition zone of the PCM oil in the proximity of the matrix/textile interface. This induces a
20 decrease in the textile reinforcement work ratio (textile efficiency ratio).



Legend : 1 Textile, 2 CSH hydrated product, 3 leaked PCM wax from damaged capsules

21

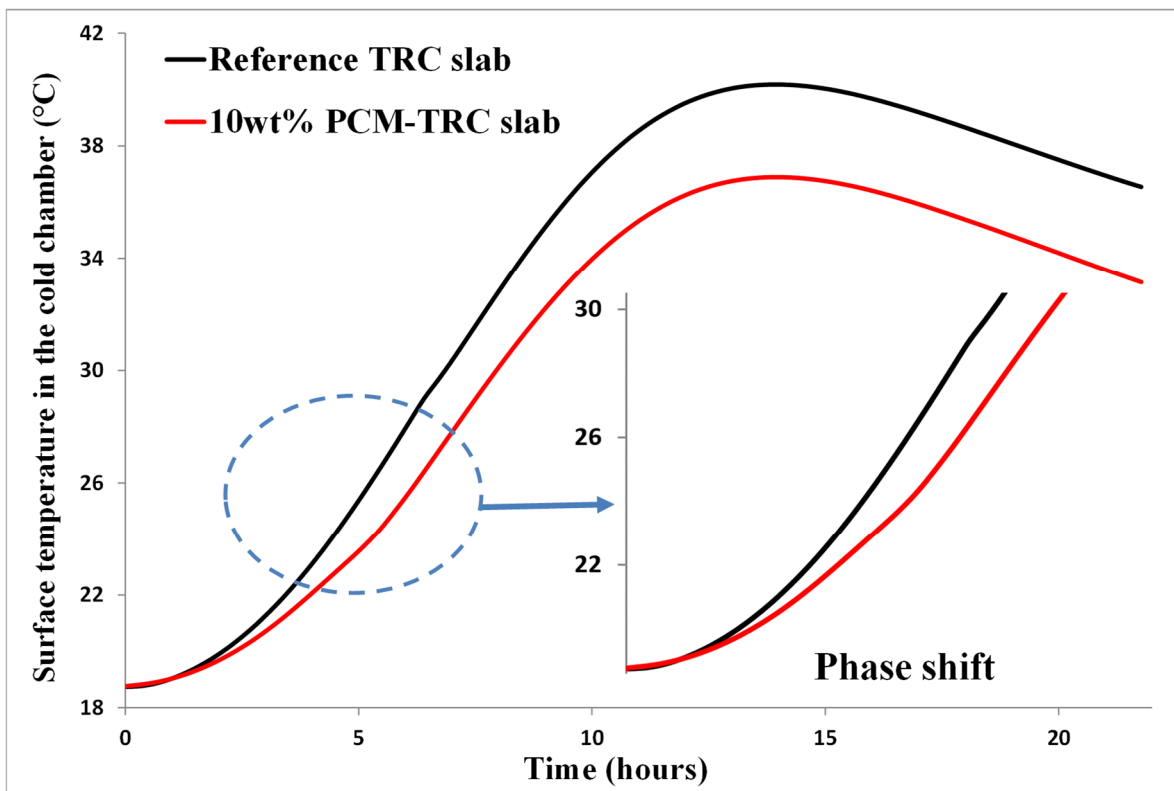
22 **Figure 19** SEM image illustrating the effect of PCM wax leakage near the interface

1

2 3-3 Thermal performances of PCM-TRC slabs (result of thermal inertia test)

3 The results of the thermal inertia test (described in **Section 2-2-4**) on the reference TRC slab
4 (without PCM) and 10wt% PCM-TRC slab (identified as the optimum balance between
5 mechanical and thermal properties) in terms of the sample surface temperature and air
6 temperature in the cold chamber are depicted in **Figures 20-a and 20-b**. Owing to the
7 complexity of the instrumentation used and the sample scale, the authors specify that the
8 results presented in this section are those obtained from a single test. The test scenario
9 involved heating from 17 to 45°C in the hot chamber while the cold chamber remained free of
10 any imposed condition.

11



12

13

-a-

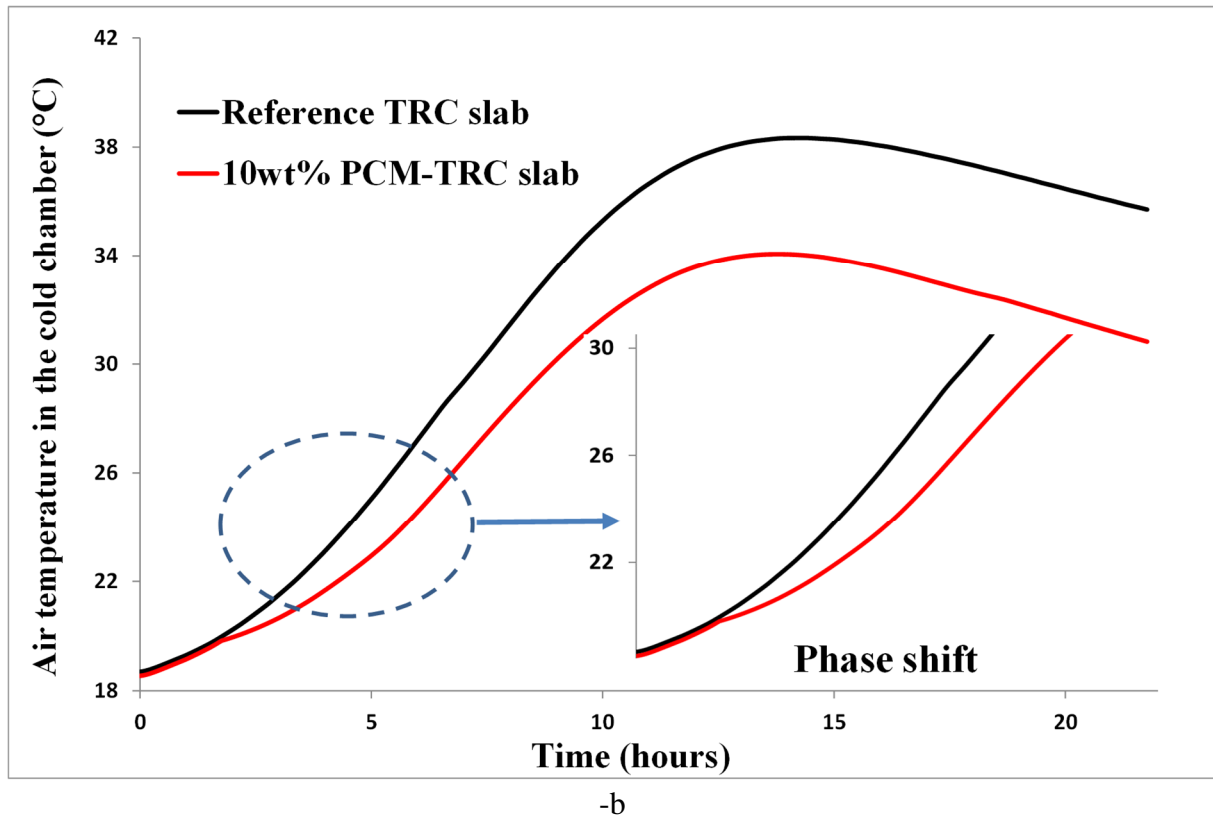


Figure 20 –a samples surface temperature **–b-** Air temperature in the cold chamber

1
2
3
4
5
6
7
8
9
10
11
12
13
14
15
16
17
18
19
20
21
22
23
24

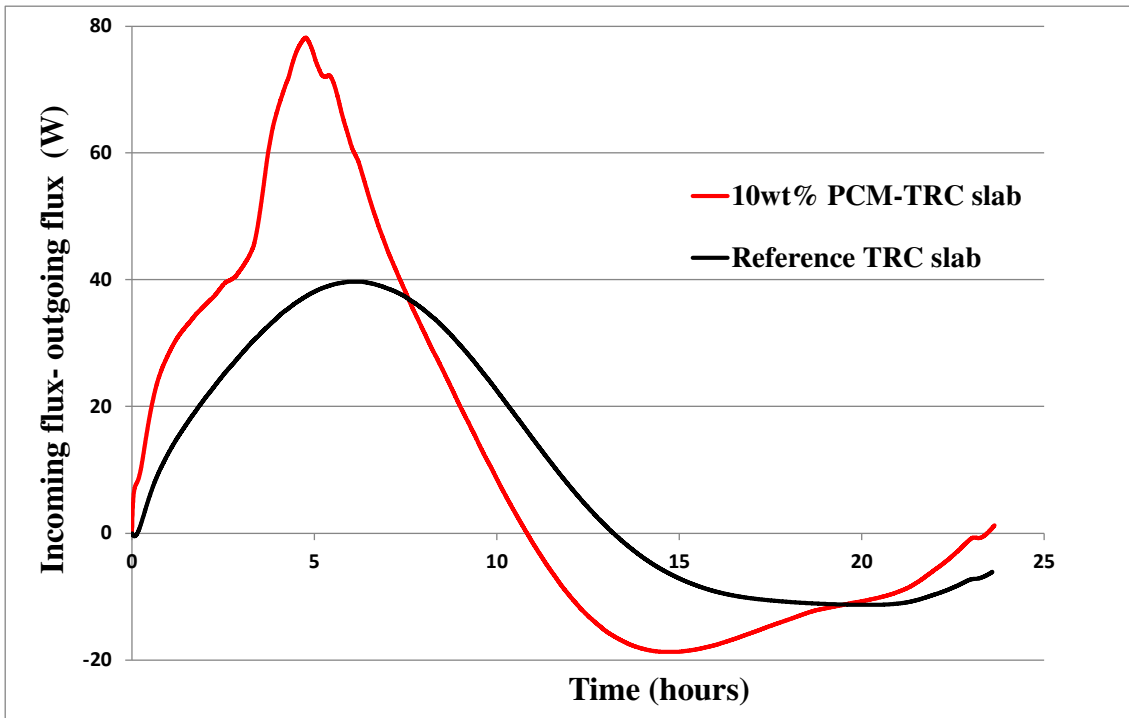
For the 10wt% PCM–TRC slab, the surface temperature in the cold chamber increased with an almost identical speed to that of the reference TRC slab in the 18.7–20°C temperature range. In contrast, when the surface temperature reached 22–27°C, a marked decrease in the speed of temperature increase was observed for the 10wt% PCM–TRC slab. This slowdown was due to the phase change (increase in specific heat of PCM and absorption of latent heat to induce phase change). The rate of temperature increase remained unchanged for the reference TRC slab.

The rate of air temperature increase in the cold chamber also demonstrated a slowing down trend in the temperature range of 20–25°C for the 10wt% PCM–TRC slab, whereas it remained unchanged for the reference TRC slab. The slight difference between the two ranges of occurrence of slowdown in temperature rise (between the indications of the surface temperature sensors and cold-side air temperature sensors) can be attributed to the heat transfer by convection from the surface of the sample to the interior air.

In comparison with the reference TRC slab during the heating process, the 10wt% PCM–TRC slab exhibited a lower surface temperature and lower air temperature at the peak. Reductions of 3.6°C in the surface temperature and 4°C in the indoor air temperature at the peak were observed. The analysis of temperature evolution also indicates a phase shift of temperature that can reach up to 3 h at the occurrence of phase change.

To compare the heat storage capacities of the reference TRC and 10wt% PCM–TRC slabs, an analysis of the heat fluxes entering the hot chamber and exiting the cold chamber for the two

1 slabs was performed. The differences between the incoming and outgoing flux in each slab
 2 are depicted in **Figure 21**.



3
 4 **Figure 21** Flux analysis in the slabs

5 The energy stored for the two slabs was evaluated by integrating the difference between the
 6 incoming and outgoing flux over the heating time. The result for each configuration is
 7 presented in **Table 8**.

Energy reference slab (kJ)	Energy 10wt% PCM-TRC (kJ)	Energy gain
2340±42	3690±60	37%

8 **Table 8** Heat storage in PCM-TRC slabs

9

10 It can be concluded after the analysis of **Figure 21** and **Table 8** that the 10wt% PCM-TRC
 11 slab presents an energy capacity gain of ~37% in comparison with the reference TRC slab.
 12 This is representing a similar gain (~37%) in terms of cooling cost (In fact, the proposed slab
 13 allows a passive use of the PCM (without the need of an energy consuming system to activate
 14 the PCM phase change). The energy capacity gain suggests that a significant part of the
 15 thermal storage capacity of the PCM is preserved, although damage occurs to some PCM
 16 capsules. This result is interesting for the future exploitation of the concept of PCM-TRC
 17 slabs. However, further studies are necessary to evaluate the efficiency of slabs on repetitive
 18 heating/cooling cycles (fatigue behavior).

19 'Furthermore, for the assessment of the energy capacity of the PCM-TRC slabs in the case of
 20 a practical use, coupled evaluation (mechanical-thermal) should be investigated. In fact, the
 21 mechanical load applied on the slabs in the service state can affect the opening of cracks due

1 to PCM phase change from solid to liquid which is likely to affect the thermal performance of
2 the slabs'

3 **3-Conclusion**

4 This paper presents an innovative concept of a PCM–TRC slab that results from the
5 association of a TRC composite with PCM microcapsules. The proposed concept is based on
6 the idea of associating the lightweight specificity of TRCs with the thermal storage capacity
7 of PCMs.

8 PCM–TRC composite slabs at different PCM rates were evaluated in terms of their
9 mechanical and thermal performances. Based on the experimental design presented above, the
10 following conclusions can be drawn:

11 -The increase in the PCM rate in the PCM–TRC slabs induced a degradation in their
12 performance in terms of load-bearing capacity.

13 -The augmentation of the PCM rate in the slabs induced a degradation in the textile work
14 ratio, and even led to a critical failure mode due to inferior matrix-to-textile bond conditions
15 that induced textile slippage from the matrix for a PCM rate of 15wt%. This can be attributed
16 to the disorders caused by PCM at the matrix/textile interface scale that induced a loss of
17 bond matrix/textile.

18 Despite the degradation of the mechanical performance of the PCM–TRC slabs with
19 increasing PCM content, the ductile and multicracking characteristics, as well as the
20 matrix/textile stress transfer behavior, remained conserved. This allowed the PCM–TRC slabs
21 to achieve load-bearing capacities at failure that were considerably greater than the force at
22 the appearance of the first crack. This is particularly interesting for the future application of
23 PCM–TRC slabs as load-bearing slabs.

24 The temperature and PCM state affect the mechanical performance of the PCM–TRC slabs.
25 Bending tests conducted on 10% PCM–TRC slabs at temperatures of 20 and 40°C
26 demonstrated that the 10wt% PCM–TRC slabs maintained and tested at 20°C exhibited a
27 higher load-bearing capacity, as well as a higher textile work ratio, than those of the slabs that
28 were heated to 40°C. This can be attributed to the cracks induced by the PCM during its phase
29 change at the interface scale. These cracks disturb the stress transfer from the matrix to the
30 interface until the textile reinforcement.

31 Further research can be undertaken to improve the mechanical performances of the PCM-
32 TRC slab. For this purpose, the optimisation of the microcapsules content (raw PCM material,
33 polymer shell of encapsulation) can be investigated to avoid the damage that can occur to
34 PCM and its harmful consequences on the matrix behaviour. Another point that could be
35 investigated, is using the pouring manufacturing technique for production of the PCM-TRC
36 composites to avoid applying any pressure on PCM.

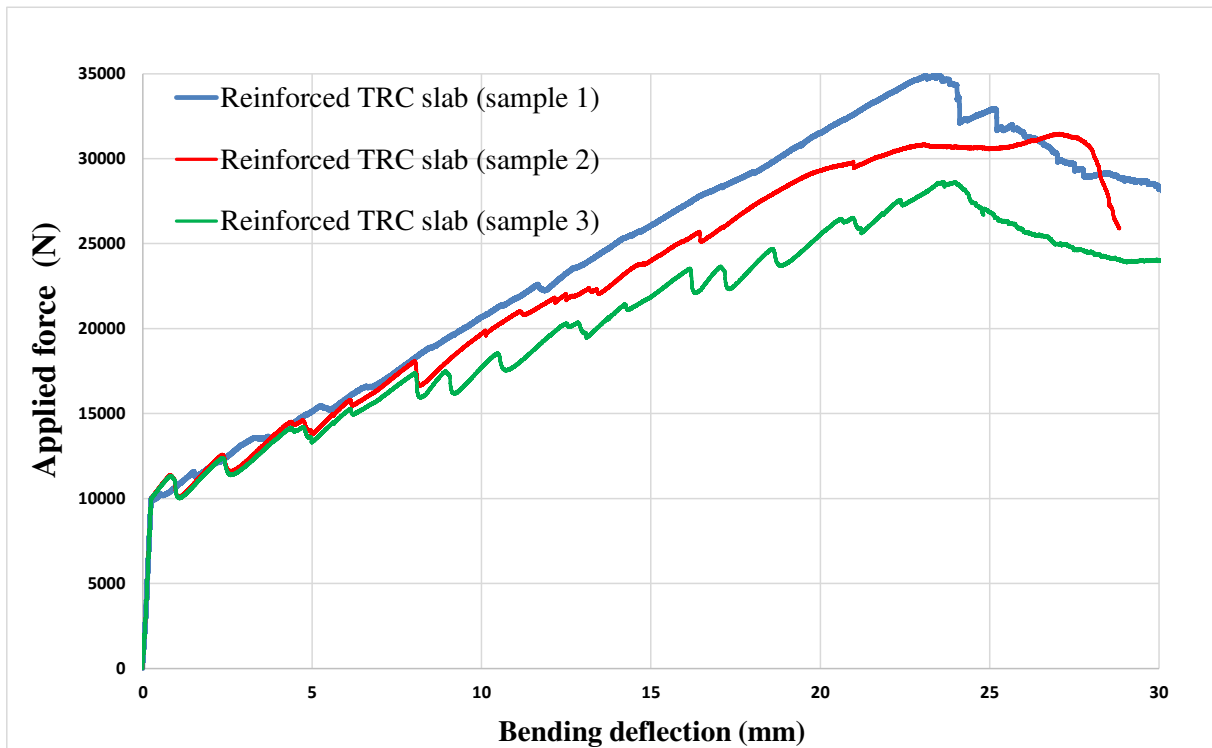
37 In terms of thermal performance, the thermal inertia of the 10 wt% PCM-TRC slab was
38 evaluated in the guarded hot box. The thermal inertia tests indicated that the 10wt% PCM–

1 TRC slab attenuated the air temperature inside the cold chamber by 4°C in comparison with
2 the reference TRC slab. The 10wt% PCM–TRC slab also allowed an increase of 37% in the
3 heat storage capacity (representing a similar saving in terms of cooling cost). This suggests
4 that a significant part of the thermal storage capacity of the PCM is preserved, although
5 damage occurs to some PCM capsules.

6 The proposed concept of PCM-TRC slabs can be very promising for the future insulation of
7 slabs in temperate climate where temperature conditions allows the PCM to ensure a full
8 cycle of phase change (solid to liquid in the morning and liquid to solid in the night).
9 However, further studies are necessary to evaluate the efficiency of the concept of PCM–TRC
10 slabs on repetitive heating/cooling cycles

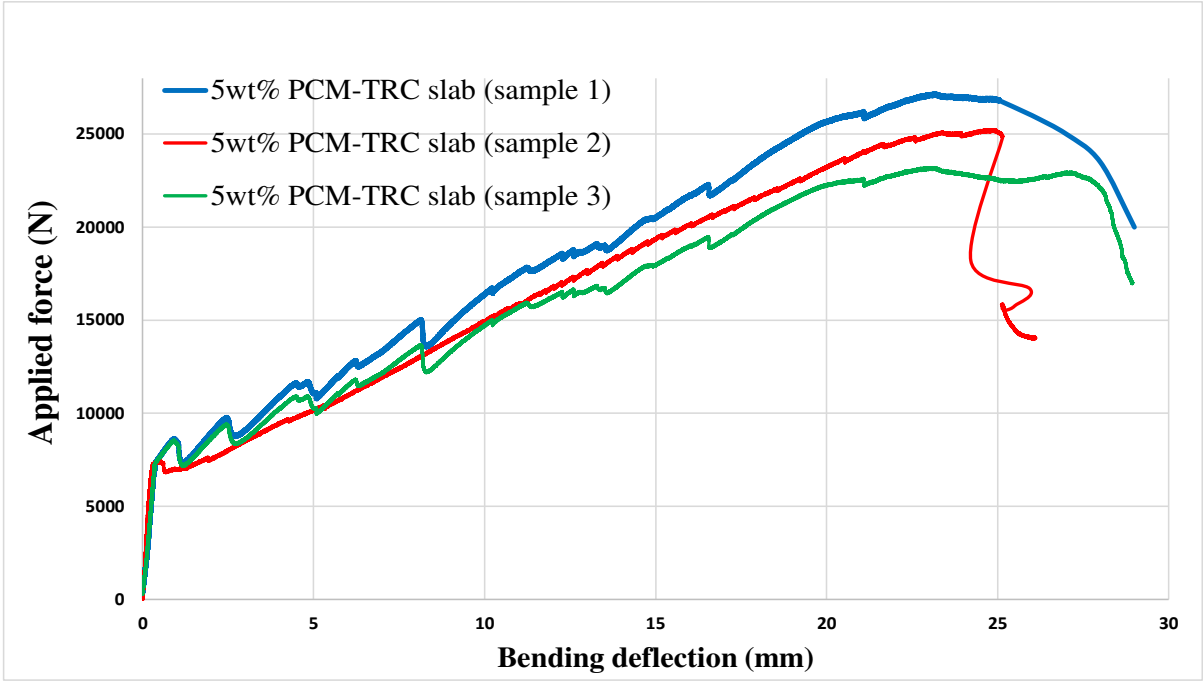
11 Appendix 1

12 All experimentally derived curves in the three points bending tests presented section 3-1-2-2
13 on three samples per PCM-TRC slab configuration (reference slab, 5wt% PCM-TRC slab,
14 10wt% PCM-TRC slab, 15wt% PCM-TRC slab) are presented below



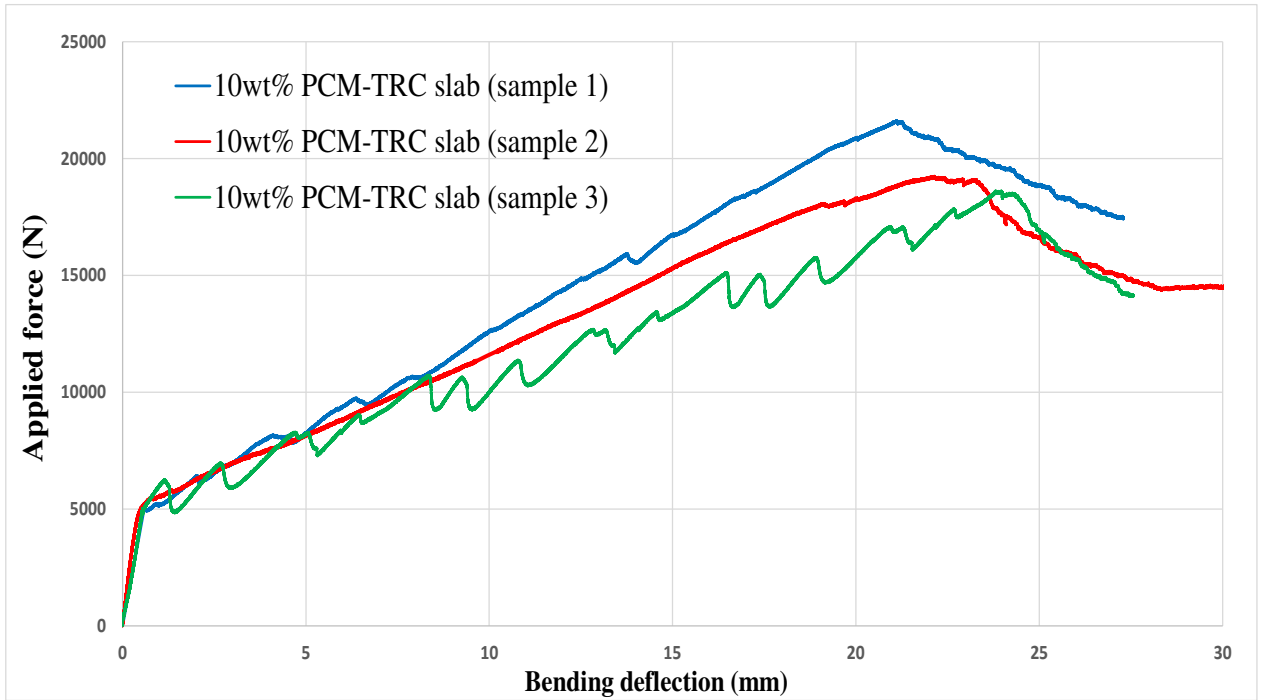
15
16

(a)



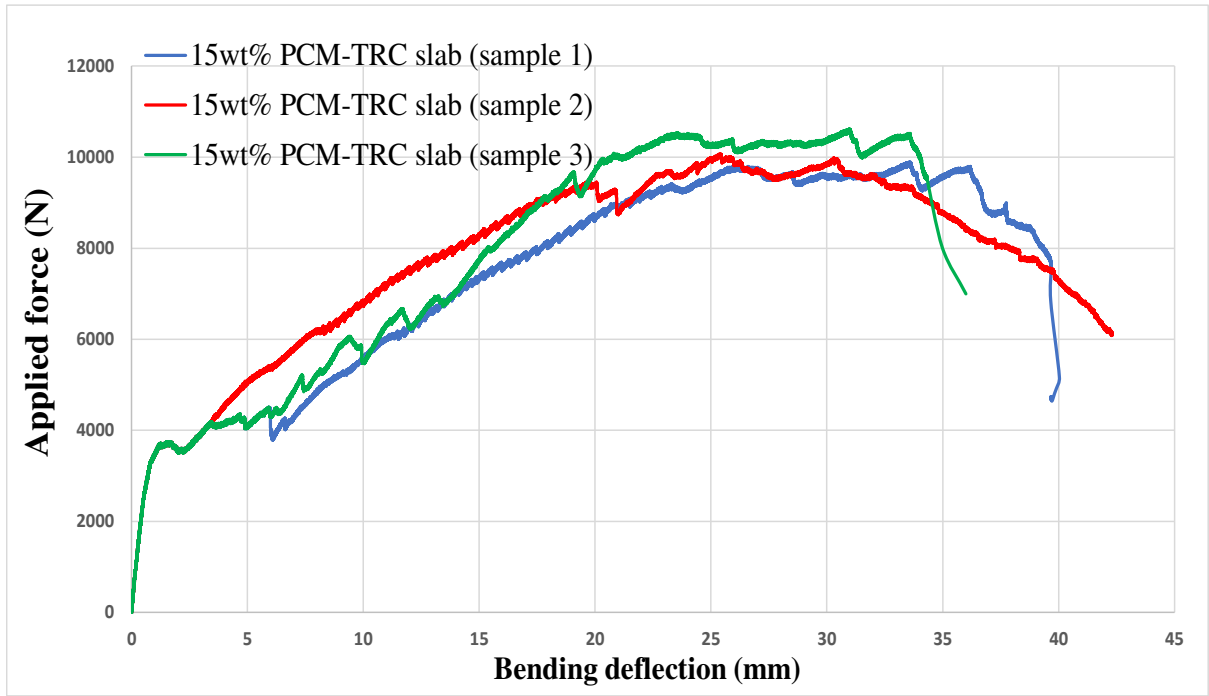
1
2

(b)

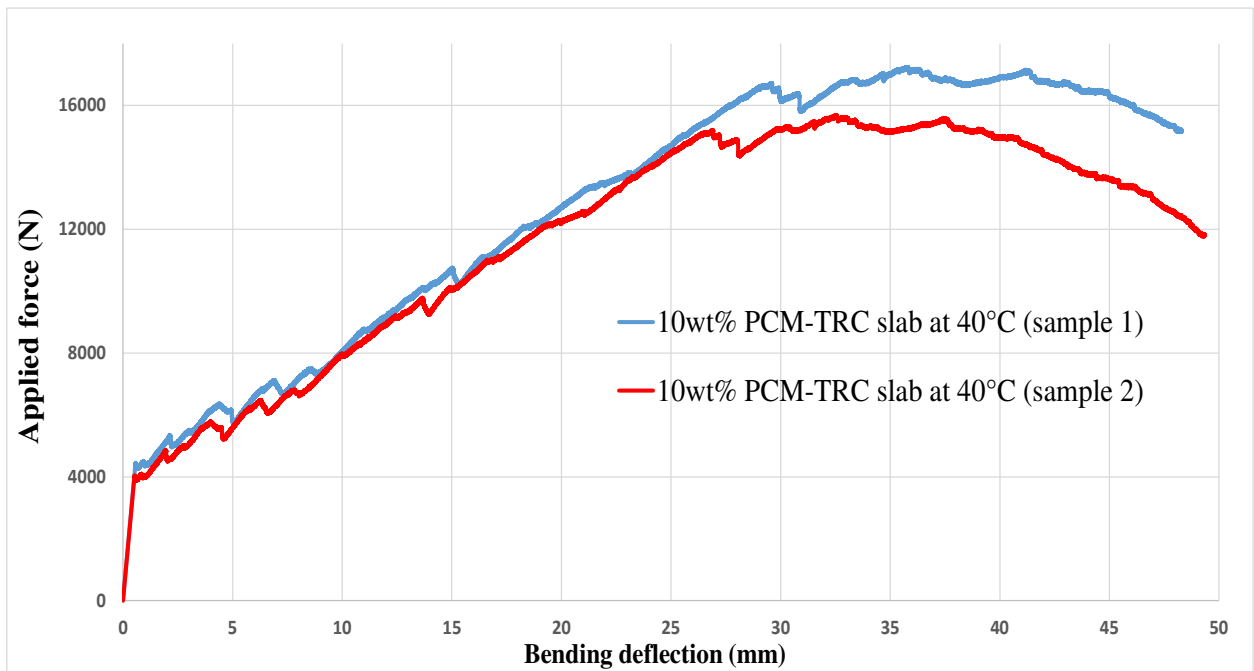


3
4
5

(c)



(d)



(d)

Figure 20 experimentally derived curves in the three points bending tests on (a) reference TRC slab (b) 5wt% PCM-TRC slab (c) 10wt% PCM-TRC slab (d) 15wt% PCM-TRC slab (e) 10wt% PCM-TRC slab at 40°C

Acknowledgement

1 The authors would like to warmly thank the company KAST (Sonthofen, Germany) for
2 providing the textile reinforcement used in the study.

3 The authors also warmly thank Mr. Bernard Arnold (KAST) for his invaluable assistance

4 **Conflicts of interests**

5 The authors have no conflicts of interests to declare.

6 **Funding:**

7 This research is funded by the Vietnam National Foundation for Science and Technology
8 Development (NAFOSTED) under grant number 107.01-2017.03.

9 The authors declare that they have no conflicts of interests.

10 **Bibliography**

11 [1] ADEME, les batiments à basse energie, retour d'experience en rhones alpes,2013.

12 [2] T D'Antino, C Papanicolaou, Mechanical characterization of textile reinforced inorganic-
13 matrix composites, Composites Part B 127 (2017) 78-91

14 [3] Z Djamai, M Bahrar, F Salvatore, A Si Larbi, M El Mankibi, Textile reinforced concrete
15 multiscale mechanical modelling: Application to TRC sandwich panels, Finite Elements in
16 Analysis and Design 135 (2017) 21-35

17 [4] J Vervloet, P Van Iterbeek, S Verbruggen, M El Kadi, M De Munck, J Wastiels,T
18 Tysmans, Experimental investigation of the buckling behaviour of Textile Reinforced Cement
19 sandwich panels with varying face thickness using Digital Image Correlation, Construction
20 and building materials, 51 (2014) 405-413

21 [5] A Shams, J Hegger, M Horstmann, An analytical model for sandwich panels made of
22 textile reinforced concrete, Construction and Building Materials 64 (2014) 451-459

23 [6] I Colombo, M Colombo, M Di Prisco, Bending behavior of textile reinforced concrete
24 sandwich beams, Construction and Building Materials 95 (2015) 675–685.

25 [7] Z I Djamai, K Erroussafi, A Si Larbi, F Salvatore, G Cai Analytical modeling of textile
26 reinforced concrete (TRC) sandwich panels: Consideration of nonlinear behavior and failure
27 modes, Mechanics of advanced Materials and structures (2020).

28 [8] J Vervloet, T Tysmans, M El Kadi, M De Munck, P Kapsalis, P Van Itterbeeck, J
29 Wastiels, D Van Hemelerijck Experimental and numerical evaluation of textile reinforced
30 cement (TRC) sandwich walls in compression: A geometrical study, Construction and
31 building Materials 240 (2020) 1-11

32 [9] L Olivieri, J Tenorio, D Revuelta, L Navarro, L Cabeza, Developing a PCM-enhanced
33 mortar for thermally active precast walls in Construction and Building Materials 181 (2018)
34 638-649

35 [10] M Pomnianowski, P heiselberg, R Jensen, R Cheng, Y Zhang, A new experimental
36 method to determine specific heat capacity of inhomogeneous concrete material with
37 incorporated microencapsulated –PCM, Cement and concrete research 55 (2014) 22-34.

- 1 [11] S Cunha, M Lima, J Aguiar, Influence of adding phase change materials on the physical
2 and mechanical properties of cement mortars, *Construction and Building Materials* 127
3 (2016) 1–10
- 4 [12] L Boussaba, A Foufa, S Makhoulf, G Lefebvre, L Royon Elaboration and properties of a
5 composite bio-based PCM for an application in building envelopes in *Construction and*
6 *building materials* 185(2018) 156-165
- 7 [13] H W Min, S Kim, H S Kim, Investigation on thermal and mechanical characteristics of
8 concrete mixed with shape stabilized phase change material for mix design, *Construction and*
9 *building materials* 149 (2017) 749-762.
- 10 [14] D Zhang, Z Li, J Zhou, K Wu, Development of thermal energy storage concrete, *Cement*
11 *and Concrete Research* 34 (2004) 927-934
- 12 [15] A Figueiredo, J Lapa, R Vicente, C Cardoso, Mechanical and thermal characterization of
13 concrete with incorporation of microencapsulated PCM for applications in thermally activated
14 slabs in *Construction and Building Materials* (2016) 126 332-344.
- 15 [16] Z Djamai, F Salvatore, A Si Larbi, G Cai, M El Mankibi, Multiphysics analysis of effects
16 of encapsulated phase change materials (PCMs) in cement mortars, *Cement and Concrete*
17 *Research* 119 (2019) 51-63.
- 18 [17] A Eddhahak-ouni, S Drissi, J colin, J Negi, S Carre, Experimental and multi-scale
19 analysis of the thermal properties of Portland cement concretes embedded with
20 microencapsulated phase change materials (PCMs), *Applied thermal engineering* 64 (2014)
21 32-39.
- 22 [18] E Mohseni, W Tang, S Wang Development of thermal energy storage lightweight
23 structural cementitious composites by means of macro-encapsulated PCM, *Construction and*
24 *Building Materials* 225 (2019)
- 25 [19] C Castellón, A Castell, M Medrano, I Martorell, L F.Cabeza Experimental Study of PCM
26 Inclusion in Different Building Envelopes, *Journal of Solar Energy Engineering* 131(2009) 1-
27 6
- 28 [20] M Hunger, A G Entrop, I Mandilaras, H J H Brookers, M Founti, The behavior of self-
29 compacting concrete containing micro-encapsulated phase change Materials, *Cement and*
30 *Concrete Composites* 31 (2009) 731–743
- 31 [21] A Thiele, A Jamet, G Sant, L Pilon, Annual energy analysis of concrete containing phase
32 change materials for building envelopes in *Energy conversion and management* 103 (2015)
33 374-386.
- 34 [22] P K Dehdezi, M R Hall, A R Dawson, S P Casey, Thermal, mechanical and
35 microstructural analysis of concrete containing microencapsulated phase change materials,
36 *Int. J. Pavement Eng.* 14 (5) (2013) 449–462.
- 37 [23] V D Cao, S Pilehvar, C Salas-Bringas, A M Szczotok, Microencapsulated phase change
38 materials for enhancing the thermal performance of Portland cement concrete and geopolymer
39 concrete for passive building applications, *Energy Conversion and Management* 133 (2017)
40 56-66.

- 1 [24] N Esside, A Loulizi, J Naji Compressive strength and hygric properties of concretes
2 incorporating microencapsulated phase change material, *Construction and building Materials*
3 22 (2019), 254-262.
- 4 [25] M Aguayo, S Das, A Maroli, N Kabay, J Mertens, S Rajan, G Sant, N. Chawla, N.
5 Neithalath, The influence of microencapsulated (PCM) characteristics on the microstructure
6 and strength of cementitious composites: Experiments and finite element simulations, *Cement*
7 *and Concrete Composites* 73 (2016) 29-41
- 8 [26] Z Djamai, A Si Larbi, F Salvatore, G Cai A new PCM-TRC composite: A mechanical
9 and physicochemical investigation, *Cement and Concrete Research* 135 (2020) 106–119
- 10 [27] S Cunha, J Aguiar, V Ferreira, A Tadeu, A Garbacz Mortars with phase change
11 materials - Part I: Physical and mechanical characterization, *Key Engineering Materials* 634
12 (2015) 22-32
- 13 [28] T Lecompte, P Le Bideau, P Glouannec, D Nortershauser, S Le Masson Mechanical and
14 thermo-physical behaviour of concretes and mortars containing phase change material, *Energy*
15 *and buildings* 94 (2015) 52-60
- 16 [29] B Savija, A Figueiredo, E Schlangen Influence of Microencapsulated Phase Change
17 Material (PCM) Addition on (Micro) Mechanical Properties of Cement Paste, *Materials* 10
18 (2017)
- 19 [30] B Savija, M Lukovic, G Kotteman, S Figueredo, F de Mendonça Filho, E Schlangen
20 Development of ductile cementitious composites incorporating microencapsulated phase
21 change materials, *International Journal of Advanced science and Applied Mathematics* 9
22 (2017) 169-180
- 23 [31] S Pilehvara, V-D Cao, A M Szczotoka, L Valentinie Mechanical properties and
24 microscale changes of geopolymer concrete and Portland cement concrete containing micro-
25 encapsulated phase change materials, *Cement and Concrete Research* 100 (2017) 341-349
- 26 [32] S Pilehvar, S Sanfelix , A Szczotok, J Rodríguez, L Valentini, M Lanzón , R Pamies , A
27 Kjøniksen Effect of temperature on geopolymer and Portland cement composites modified
28 with Micro-encapsulated Phase Change materials
- 29 [33] Zakaria Ilyes DJAMAI Phd thesis Contribution à la caractérisation multi-échelle de
30 composites textile mortier à inertie thermique renforcée par des matériaux à changement de
31 phase (composite MCP-TRC) : application au bâtiment
- 32 [34] M Felix, J Aguiar Study of a cement mortar with incorporation of PCM microcapsules in
33 proceeding of the 6th symposium of polymers in concrete, Shanghai China
- 34 [35] European norm: methods of testing cement. Determination of strength
- 35 [36] Test method for steady-state thermal performance of building assemblies by means of a
36 guarded hot box

37

38